Journal of Progress in **Engineering and Physical Science**

Volume 5, Number 1 **March 2026**

CONTENTS

Journal of Progress in Engineering and Physical Science
ISSN 2709-4006
www.paradigmpress.org/jpeps
Volume 5 Number 1 March 2026

Response to "Cosmological Consequences of the Lorentz and Doppler Transformations"

A. Sfarti[1]

[1] CS Dept, UC Berkeley, 387 Soda Hall, Berkeley, CA, USA
Correspondence: A. Sfarti, CS Dept, UC Berkeley, 387 Soda Hall, Berkeley, CA, USA.

doi:10.63593/JPEPS.2026.03.01

Abstract

The paper "Cosmological Consequences of the Lorentz and Doppler Transformations" by Vaclav Vavryčuk claims that the Lorentz transformation's physical interpretation is flawed and advocates for a "Doppler metric" instead of the standard Minkowski metric as a better description of spacetime distortion, an idea that contradicts the well-established foundation of Einstein's Special Relativity and is not supported by mainstream physics.

Keywords: Minkowski metric, Lorentz metric, Michelson-Morley experiment, preferred reference frame, relativistic time dilation

---

Contradicts established physics: The paper claims the common physical interpretation of the Lorentz transformation is flawed, which undermines a cornerstone of modern physics, Special Relativity.

Proposes a new metric: It introduces a new "Doppler metric" as more appropriate for describing spacetime distortion, an idea that goes against the established Minkowski metric.

Misinterprets the results of the Michelson-Morley experiment: The paper's claims about how experiments like the Michelson-Morley experiment support its Doppler metric are in effect a misinterpretation of mainstream physics. The paper claims that the null result of the Michelson–Morley experiment did not fail to detect the existence of a preferred reference frame and it suggests the null result of the experiment is explained by the Doppler effect canceling out.

Advocates for a preferred reference frame: The paper and related works argue that cosmological observations, specifically the Cosmic Microwave Background (CMB) dipole anisotropy, indicate a preferred, stationary reference frame. This directly contradicts a core tenet of Special Relativity, which posits that all inertial frames are equivalent and there is no universal, preferred frame of reference. This exact claim about the frame in which CMBR dipole anisotropy is null is a preferred frame for relativity is not new, other fringe papers have claimed that before and have been refuted.

Claims resolution of several cosmological problems: The paper asserts that its reinterpretation can resolve some challenges to the standard Lambda-CDM cosmological model, including observations of supernova dimming and flat galactic rotation curves.

Here is a side by side comparison between the mainstream data and the paper claims.

Table 1.

Element	Paper's Claim	Mainstream Physics Consensus
Lorentz Transformations	The paper argues that the conventional interpretation of Lorentz transformations is flawed and that time dilation and length contraction are eliminated when non-diagonal terms are handled differently. The paper states this would make the Lorentz metric identical to the Minkowski metric (sic!).	The Lorentz transformations are the cornerstone of special relativity. The standard interpretation is that they produce real physical effects of time dilation and length contraction for observers in relative motion.
"Doppler Metric"	A "Doppler metric" is introduced to describe spacetime distortion in moving inertial frames and is linked to the Doppler shift of light. The paper claims this metric requires a preferred reference frame.	The standard model uses the Minkowski metric to describe spacetime in special relativity. General relativity is metric-based, but does not include a "Doppler metric" as described.
Preferred Reference Frame	The paper assumes the existence of a special, or "preferred," reference frame in the universe. It points to observations of the Cosmic Microwave Background (CMB) dipole anisotropy to support this, claiming it detects a measurable drift relative to this frame.	Special relativity, a foundation of modern physics, asserts that the laws of physics are the same for all inertial observers and that there is no preferred reference frame.
Michelson-Morley Experiment	The paper reinterprets the results of the Michelson-Morley experiment, arguing its null result is an inherent limitation of the experimental setup due to the Doppler effect, and does not rule out the existence of a luminiferous aether.	The null result of the Michelson-Morley experiment is one of the foundational experiments that demonstrated the non-existence of the luminiferous aether and helped establish the principles of special relativity.
Dark Matter and Dark Energy	The paper and its related work claim that this conformal cosmology approach can explain observations without the need for dark matter or dark energy.	Mainstream cosmology, primarily the Lambda-CDM model, relies on the concepts of dark matter and dark energy to explain observational evidence like galaxy rotation curves and the accelerated expansion of the universe.

There are also several serious computational errors in the paper:

The failed attempt at computing time dilation from the Lorentz transform of time: The correct way is to simply differentiate the transform for time and to impose the condition of locality ($dx = 0$) and the author does not understand this basic fact:

$$dt' = \gamma(dt - \frac{vdx}{c^2})|_{dx=0} = \gamma dt$$

Instead, the author obtains $dt'/dt = 1$ (author's equation 10). This flies in the face of all the Ives-Stilwell experiments that have verified (since 1938) the reality of time dilation. The author claims that the mainstream derivations of time dilations are all "flawed":

"Surprisingly, Eq. (17) predicts a varying proper speed of light. This implies that the Lorentz transformation itself (defined in Eq. (5)) is consistent with the SR postulate of the constant speed of light, the derivation of time dilation from the Lorentz transformation in Eq. (11) is flawed. Equation (11) is thus inconsistent with the Lorentz transformation as

well as with the SR postulate of the constant speed of light c."

The failure in computing proper speed of light: The error is tracked to the incorrect computation of the metric (author equation 14) where there is an incorrect presence of the γ^{-2} instead of the correct γ^{2} producing the incorrect $C = \gamma c$ (author's equation 17) instead of recognizing that the metric is frame invariant, thus recovering c as the proper light speed, a fact known since demonstrated by Einstein in 1905.

In conclusion, there are too many fundamental errors in the published paper.

References

V. Vavryčuk. (2024). Cosmological consequences of the Lorentz and Doppler transformations. *Modern Physics Letters A*, *39*(Nos. 21 & 22), 2450098.

Appendix

The "review" from the MPLA assigned reviewer https://drive.google.com/file/d/1h32XyIEj7Zjf8M8ZsM4cLWJdi9h5k-WR/view?usp=drive_link

Journal of Progress in Engineering and Physical Science
ISSN 2709-4006
www.paradigmpress.org/jpeps
Volume 5 Number 1 March 2026

Application of Wi-Fi Devices for Signal Processing to Send and Receive Data

Chenglu Zhou[1]

[1] CATs College, University of Cambridge, Cambridge, United Kingdom
Correspondence: Chenglu Zhou, CATs College, University of Cambridge, Cambridge, United Kingdom.

doi:10.63593/JPEPS.2026.03.02

Abstract

This paper examines the implementation of Wi-Fi devices in signal-processing methods to transmit and receive data reliably in complex wireless networks. It describes radio signal mechanisms at the physical layer for transmitting digital information and decoding it at the other end, accounting for noise, interference, and multipath fading. Such technologies as Orthogonal Frequency Division Multiplexing (OFDM), Multiple-Input Multiple-Output (MIMO), and Channel State Information (CSI) are examined to demonstrate how contemporary Wi-Fi systems become very fast and powerful. It also discusses how these signal-processing techniques support uses like Wi-Fi sensing, security surveillance, and health tracking.

Keywords: Wi-Fi, signal processing, OFDM, MIMO, CSI, physical layer, multipath fading, Wi-Fi sensing, wireless security, health monitoring

1. Introduction

Wi-Fi is a wireless technology through which gadgets such as laptops, smartphones, and routers communicate through radio waves. Wi-Fi networks are electromagnetic networks rather than physical cables that transfer electrical impulses; the data is received by a receiver. These radio waves are sent in a very noisy environment with the reflections of walls and other objects, as well as other wireless devices. Such impairments require more than just transmission and reception to establish effective communication; this requires more sophisticated signal processing devices at both ends of the connection.

With a Wi-Fi transmitter, the sender encodes binary data, which is then converted into a radio channel, which undergoes modulation and occupies a radio frequency channel. This signal spreads to the receiver, having been corrupted by multipath fading, attenuation, and noise. To get back the data sent the receiver needs to estimate how the channel has distorted the signal and adjust those distortions. It entails modulation, channel estimation, filtering, and decoding, which are applied to the physical (PHY) layer of Wi-Fi devices (Paul & Ogunfunmi, 2008; Harkat et al., 2022).

Modern Wi-Fi is efficient and robust due to three major technologies, namely Orthogonal Frequency Division Multiplexing (OFDM), Multiple-Input Multiple-Output (MIMO), and

Channel State Information (CSI). OFDM splits the bandwidth into a large number of narrow subcarriers to be less sensitive to multipath distortion, MIMO employs multiple antennas to capitalize on spatial diversity and transmit many data streams, and CSI measures the wireless channel effects on the signal in great detail. A combination of these methods enables Wi-Fi systems to adjust to the dynamic radio conditions and ensure high data throughput.

2. Wi-Fi Transmission and Reception

The Wi-Fi communication starts with digital data, which can be a webpage or video, which is a stream of bits. These bits have to be encoded into a radio channel transmission waveform. This is converted in the Wi-Fi physical layer that carries out channel coding, modulation, and generation of waveforms (Paul & Ogunfunmi, 2008).

Error-correcting codes are performed at the transmitter, at which point the receiver is able to detect and correct bit errors due to noise and interference. The coded bits are then mapped onto the modulation symbols, like QPSK or QAM, which are various values of amplitude and phase. They are the symbols allocated to the subcarriers of the OFDM, and an inverse Fourier transform is employed to create a time domain signal. This is translated to an analog radio signal and broadcast with the antenna.

The signal sent by the transmissions flows through the wireless medium through which it experiences attenuation, noise, and multipath distortion. When in an interior setting, the signal is reflected at the walls, furniture, and individuals, and thus, the receiver will receive several delayed copies of the signal. These overlapping copies introduce frequency-selective fading, i.e., certain areas of the spectrum are weaker as compared to others (Harkat et al., 2022).

The antenna at the receiver picks up a distorted signal. The receiver initially matches the transmitting signal and trims the cyclic prefix that was appended during the transmission of the OFDM signal. The preamble in the packet contains known training symbols, which are then used to estimate the channel. This estimate enables the recipient to balance all the subcarriers, which redresses the effects of fading and distortion. With equalization, the subcarriers are demodulated again into digital symbols and decoded to obtain the original bitstream.

With this transmit-receive channel process, it can be seen that Wi-Fi relies on the constant monitoring and correction of the radio signal through signal processing and not by direct broadcast.

3. OFDM in Wi-Fi

Orthogonal Frequency Division Multiplexing (OFDM) is the modulation scheme of new generations of Wi-Fi standards like IEEE 802.11a, 802.11n, and others. OFDM breaks down the spectrum available into a large number of subcarriers, which are spread closely and carry a share of the data. These subcarriers are mathematically orthogonal; thus, they can overlap in frequency and not interfere with each other (Harkat et al., 2022).

The foremost strength of the OFDM is that it is resistant to distortion by multipaths. Inter-symbol interference in single-carrier systems is due to delayed signal copies that reduce the performance of the system. In the OFDM, many narrowband subcarriers are used to transmit each symbol, thus the symbol period is long relative to normal multipath delays. After each OFDM symbol, a cyclic prefix is inserted to avoid the interference of the main signal by echoes.

A Fourier transform is used at the receiver to split the signal received into subcarriers. Independent equalization of each subcarrier can then be done based on the channel estimate. It is now possible to compensate for frequency-selective fading, in which various regions of the spectrum are subjected to varying attenuation.

Hernandez and Bulut (2022) state that fine-grained frequency-domain information about the wireless channel is also available under OFDM and can be used to channel estimate and higher-layer processing. This is the reason why Wi-Fi communication and Wi-Fi-based sensing rely on the basic principles of OFDM.

4. MIMO in Wi-Fi

Wi-Fi modern systems include a variety of features that are based on Multiple-Input Multiple-Output (MIMO). MIMO applies multiple transmit and receive antennas in place of one antenna in order to enhance data throughput and link reliability. Standards derived under the IEEE 802.11n up to IEEE 802.11ng are capable of supporting MIMO space multiplexing, space-time block coding, and beamforming (Paul & Ogunfunmi, 2008).

In spatial multiplexing, the data streams of

various antennas are sent at the same frequency band but via different antennas. Due to the fact that propagation of each of the streams takes place across slightly different wireless channels, the receiver is able to isolate the streams by channel estimation and signal processing. This multiplies the data rate without the need to add more bandwidth.

MIMO also uses beamforming, whereby the transmitter tunes the phase and amplitude of signals in its antennas so that they can constructively add at the receiver. This enhances signal strength and eliminates interference. Space-time block coding offers diversity relaying redundant information over two or more antennas, and this is beneficial in fading conditions.

Harkat et al. (2022) note that MIMO-OFDM systems need to estimate and equalize channels correctly to decipher and decode several spatial streams. This also shows that the Wi-Fi devices are actually real-time signal processors, which constantly examine the wireless channel to maximize performance.

5. Channel State Information (CSI)

Channel State Information (CSI) is the description of the radio channel propagation of a wireless signal between a transmitter and a receiver. CSI in Wi-Fi networks with MIMO and OFDM is described as a complex-valued matrix that describes the attenuation and phase shift of each subcarrier in every pair of transmit and receive antennas (Ma, Zhou, & Wang, 2019). CSI, as opposed to coarse metrics like Received Signal Strength Indicator (RSSI), reflects finer-grained frequency-domain and spatial channel response.

Every CSI value comprises both an amplitude component and a phase component. The amplitude is the amount that has been attenuated by the channel, and the phase is the delay and the path length due to multiple path propagation. When CSI is viewed across subcarriers, frequency-specific fading is apparent, with some frequencies deep-fading (frequent) and others strong (Ma et al., 2019). Since Wi-Fi applies the OFDM, CSI is calculated per subcarrier, so one can model the channels fine-granularly.

CSI is vital to a stable Wi-Fi communication because it allows the receiver to rectify the distortion of the channel, and allows advanced techniques, such as beamforming and spatial multiplexing. According to Gringoli et al. (2019), when a frame preamble is received, the CSI is estimated to equalize the remaining data symbols. CSIS feedback to the transmitter can also be sent to adjust its transmission strategy, such as the choice of beamforming weights or the choice of MIMO mode.

There are pre-established training symbols in Wi-Fi packet preambles to compute CSI. Halperin et al. (2011) add that the IEEE 802.11n receiver uses known long training symbols (LTFs) to ascertain the channel frequency response. The model below provides the received signal on each subcarrier:

$$y = Hx + n,$$

where,

x is the transmitted symbol, y is the received symbol, H is the CSI matrix, and n is noise. Using the received y and the known x, the receiver decides the estimation of H per subcarrier and antenna pair. This CSI is then used by the equalizer to undo channel distortion and is then demodulated.

6. The Signal Processing at the Receiver

The Wi-Fi receiver uses a set of signal processing to reconstruct the message sent by a mangled and noisy radio signal. Noise and interference mitigation is the first phase, during which filtering, timing, and frequency alignment are used to eliminate out-of-band noise and synchronize the receiver with the timing and frequency of the transmitter (Hernandez & Bulut, 2022).

The estimation of the channels is then done through CSI. The packet preamble includes training symbols that the receiver uses to calculate the frequency response of the wireless channel of each OFDM subcarrier. Equalization is applied to this channel estimate to correct attenuation of amplitude and phase distortion to ensure that the received signal is more similar to the one sent (Yang et al., 2022).

Upon equalization, demodulation is done by the receiver to recover the complex OFDM symbols in the form of digital symbol values. These codes are decoded by means of error correcting decoders like convolutional decoders, LDPC decoders, etc., to reconstruct the original bitstream. This last step removes remnant errors due to noise, fading, or interference (Hernandez & Bulut, 2022).

More recent work has been done on receiver processing with deep learning. As demonstrated by Wang et al. (2023), convolutional neural

networks are capable of training the mapping between received signals, which are noisy, and sent signals, which reduces bit-error rate in noisy impulsive receiver settings. It proves that recent Wi-Fi receivers are moving towards a combination of more traditional signal processing and data-driven algorithms.

7. Current uses of Wi-Fi Signal Processing

In addition to data communication, Wi-Fi signal processing also allows numerous sensing and monitoring applications. Since CSI measures finer details of signal propagation, it can be employed to monitor environmental changes without the need to install more sensors.

Wi-Fi sensing may sense human presence, gestures, and patterns of activities to control the appliances without the devices in smart homes (Ma et al., 2019; Yang et al., 2022). In security and motion detection, the variation of the amplitude and phase of the CSI signal detects motion, and the Wi-Fi system can detect intrusions even through the walls.

CSI variations have been applied in health monitoring in order to monitor respiration rate, falls, and human activity. Ma et al. (2019) demonstrate that the patterns of breathing and motion are present in the CSI time series, allowing non-contact monitoring of the vitals. Hernandez and Bulut (2022) also show that these signal processing pipelines can execute on low-priced embedded Wi-Fi gadgets.

These applications are based on the same OFDM, MIMO, and CSI technologies that facilitate data transmission, which underscores the dual nature of Wi-Fi as a communication and sensing platform.

8. Difficulties and Future Enhancement

The noise, interference, and hardware limitations are some of the problems that hinder Wi-Fi signal processing. Saturated wireless space brings about the problem of co-channel interferences whereas the low-cost hardware reduces sampling rate and computing capabilities (Hernandez & Bulut, 2022). Multi-path fading and noise of impulse further decrease reliability.

A potentially successful direction is the processing of AI. Wang et al. (2023) show that deep learning is more effective in a high noise environment than traditional receivers, meaning that the next generation of Wi-Fi systems will combine traditional signal processing with neural networks to be stronger and more efficient.

9. Conclusion

The Wi-Fi is not simply a radio connection, but a more sophisticated signal-processing system. OFDM divides the spectrum into subcarriers, which are easily manageable; MIMO leverages the diversity in space, and CSI provides more channel knowledge. Combined, these technologies enable Wi-Fi devices to be flexible to changing environments, to be used in providing high-speed communications, and to be used in sensing applications. With the further development of signal processing and AI, Wi-Fi will be one of the underlying technologies in connectivity and smart spaces.

References

Gringoli, F., Schulz, M., Link, J., & Hollick, M. (2019). Free your CSI: A channel state information extraction platform for modern Wi-Fi chipsets. *Proceedings of the 12th International Workshop on Wireless Network Testbeds, Experimental Evaluation & Characterization (WiNTECH 2019)*. https://doi.org/10.1145/3349623.3355477

Halperin, D., Hu, W., Sheth, A., & Wetherall, D. (2011). Tool release: Gathering 802.11n traces with channel state information. *ACM Computer Communication Review, 41*(1), 53.

Harkat, H., Monteiro, P., Gameiro, A., Guiomar, F., & Ahmed, H. F. T. (2022). A survey on MIMO-OFDM systems: Review of recent trends. *Signals, 3*(2), 359-395. https://doi.org/10.3390/signals3020023

Hernandez, S. M., & Bulut, E. (2022). WiFi sensing on the edge: Signal processing techniques and challenges for real-world systems. *IEEE Communications Surveys & Tutorials, 24*(2), 1230-1260. https://doi.org/10.1109/COMST.2022.3209144

Ma, Y., Zhou, G., & Wang, S. (2019). WiFi sensing with channel state information: A survey. *ACM Computing Surveys, 52*(3), 1-36.

Paul, T., & Ogunfunmi, T. (2008). Wireless LAN comes of age: Understanding the IEEE 802.11n amendment. *IEEE Circuits and Systems Magazine, 8*(1), 28-54. https://doi.org/10.1109/MCAS.2008.915504

Wang, B., Jiang, Z., Sun, Y., & Chen, Y. (2023). An intelligent signal processing method against impulsive noise interference in AIoT.

EURASIP Journal on Advances in Signal Processing, 2023(104), 1-18. https://doi.org/10.1186/s13634-023-01061-8

Yang, Z., Zhang, Y., Chi, G., & Zhang, G. (2022). Hands-on wireless sensing with Wi-Fi: A tutorial. arXiv:2206.09532.

Journal of Progress in Engineering and Physical Science
ISSN 2709-4006
www.paradigmpress.org/jpeps
Volume 5 Number 1 March 2026

Deep Integration of Sensing Technology and Smart Manufacturing: Leading the Technological Upgrade of the Precision Manufacturing Industry

Huajun Liu[1]

[1] Shenzhen Fanhua Wuchuang Technology Co., Ltd., Shenzhen 518000, China
Correspondence: Huajun Liu, Shenzhen Fanhua Wuchuang Technology Co., Ltd., Shenzhen 518000, China.

doi:10.63593/JPEPS.2026.03.03

Abstract

Aiming at the technical bottlenecks in core links of the precision manufacturing industry, such as ultra-precision measurement and flexible production—including insufficient machining accuracy (traditional machining error ≥±0.025 μm), response lag (process adjustment delay >100 ms), and data silos—this paper proposes a full-chain integrated architecture of "perception-modeling-decision-execution". It reveals the signal crosstalk mechanism of multi-physics field coupled sensing units and systematically elaborates the deep collaboration mechanism between multi-parameter collaborative perception and digital twin, AI adaptive control, and industrial interconnection. By developing a four-parameter integrated MEMS sensing module based on frequency domain isolation, an attention mechanism-improved LSTM algorithm, and a cross-protocol adaptive conversion middleware, three core technological breakthroughs are achieved: (1) The measurement accuracy is improved from ±0.025 μm to ±0.006 μm (a relative increase of 76%), with a complex surface detection error ≤4.2 μm; (2) The response delay is reduced from >100 ms to 0.8 ms (a reduction of 99.2%), and the equipment fault early warning accuracy reaches 94.7%; (3) The changeover efficiency of flexible production lines is increased by 45%, and the product defect rate is reduced from 3.2% to 0.5% (a reduction of 84.4%). Empirical verification in three typical industrial scenarios shows that the integrated system increases production efficiency by 32%-48% and reduces comprehensive manufacturing costs by 18%-26%. The research results provide a systematic solution for the transformation of the precision manufacturing industry. Relevant technologies have formed 15 authorized patents and 11 software copyrights, possessing significant academic value and industrial application prospects.

Keywords: multi-parameter MEMS composite sensing, attention LSTM, weighted ICP, cross-protocol conversion, precision manufacturing, digital twin

1. Introduction

1.1 Research Background and Industrial Demand

The global precision manufacturing market size reached 782 billion US dollars in 2024, with a compound annual growth rate of 12.8% (Grand View Research, 2024). High-end industries such as aerospace and semiconductors have

demanded nanoscale machining accuracy (≤±0.01 μm) (Pomeas, 2024; Liu C, et al., 2024). As the core perception component of smart manufacturing, current sensor applications face four major pain points: (1) Single-parameter detection cannot cover multi-physical quantity collaborative monitoring, with a synchronization error of >50 μs in discrete solutions; (2) Precision attenuation ≥10% under extreme working conditions, failing to adapt to the processing of aerospace components; (3) Data transmission and processing delay exceeding 100 ms, leading to lagging process adjustments; (4) Protocol incompatibility resulting in a data interaction rate of less than 60% (Chen W. & Liu J., 2023; Schmidt M, et al., 2019). According to a Deloitte report, related issues cause annual economic losses exceeding 50 billion US dollars (Deloitte, 2024). Constructing a deeply integrated system of sensing and smart manufacturing has become the key to technological upgrading.

1.2 Research Status at Home and Abroad and Research Gap

In the field of ultra-precision measurement, the axial resolution of spectral confocal sensors reaches 0.006 μm (Pomeas, 2024), and the fusion scheme of lidar and vision achieves a detection rate of >99% (Chen W. & Liu J., 2023); in process monitoring, the linearity error of force-sensitive array sensors is <3% (Chen W. & Liu J., 2023). In terms of integration technology, the combination of digital twin and sensing data increases turbine disk processing efficiency by 20% (Liu C, et al., 2024; Schmidt M, et al., 2019), and AI-driven predictive maintenance achieves an early warning accuracy of over 85% (Chen W. & Liu J., 2023). However, existing research has limitations: MIT's multi-parameter sensing module only supports 2 types of parameters with a volume >5 cm^3 (Rus D, et al., 2023); Stanford's AI algorithm has an inference time ≥50 ms (Zhang Y, et al., 2024); domestic research lacks full-chain architecture design and fails to solve the problem of precision stability under extreme working conditions (Liu J, et al., 2024).

Core Research Gaps: (1) Insufficient miniaturization and synchronization of multi-parameter integration, with a synchronization error >20 μs; (2) Unclear precision attenuation mechanism under extreme working conditions, with attenuation ≥10%; (3) End-to-end response delay exceeding 100 ms; (4) Digital twin mapping error >8% (Chen W. & Liu J., 2023; Schmidt M, et al., 2019).

1.3 Research Objectives and Innovations

This paper constructs an integrated system of "multi-sensor fusion-edge intelligence-industrial interconnection-digital twin", with the following core innovations:

(1) Four-parameter collaborative perception technology: Reveal the multi-physics field coupled crosstalk mechanism, propose frequency domain isolation and spatial layout optimization methods. To the best of our knowledge, temperature/pressure/vibration/morphology four parameters are integrated on a single MEMS chip for the first time, with a volume of 1.5 cm^3, synchronization error ≤5 μs, and precision attenuation ≤3% under extreme working conditions.

(2) Attention LSTM algorithm: Aiming at the non-stationary characteristics of industrial time series, propose an adaptive feature extraction mechanism to solve the gradient attenuation problem of standard LSTM. The computational complexity is $O(T \cdot d^2)$ (T is the sequence length, d is the feature dimension), with an early warning accuracy of 94.7% and an inference time of 187 μs.

(3) Cross-protocol conversion middleware: Realize seamless conversion of three major protocols based on a state machine, with a data interaction rate of 98% and a transmission delay ≤12 μs. Reliability is guaranteed through formal verification.

(4) Weighted ICP mapping algorithm: Derive the optimal weight function and convergence conditions, reduce the number of registration iterations by 39.9%, achieve a mapping error ≤3%, and an update frequency ≥100 Hz.

1.4 Paper Structure

Chapter 2 elaborates the integrated system architecture and core technical principles; Chapter 3 introduces the implementation of key technologies; Chapter 4 verifies performance through experiments; Chapter 5 compares with existing technologies; Chapter 6 summarizes and prospects future directions.

2. Overall Architecture and Core Technical Principles of the Integrated System

2.1 Overall Integrated Architecture Design

A four-layer integrated architecture of "perception layer-edge layer-interconnection layer-application layer" is constructed. Through functional collaboration and data closed-loop at all levels, full-chain optimization of "data

collection-preprocessing-transmission-decision-execution" is realized. The core functions, key technical schemes, and performance indicators of each layer are shown in the following table:

Table 1. Detailed Description of the Four-Layer Integrated System Architecture

Architecture Layer	Core Functions	Key Technical Schemes	Core Performance Indicators	Hardware Support
Perception Layer	Four-parameter synchronous collection, anti-interference data acquisition, multi-physics field signal isolation	1. MEMS integration technology with frequency domain isolation and spatial layout optimization; 2. FPGA 100 MHz global clock synchronization; 3. Ceramic packaging + shielded wiring + differential transmission; 4. PTFE waterproof and breathable membrane for humidity protection	1. Multi-parameter collection synchronization error ≤5 μs; 2. Precision attenuation ≤3% in wide temperature range (-40℃~150℃); 3. Signal signal-to-noise ratio ≥45 dB; 4. Module volume ≤1.5 cm^3	Multi-parameter composite sensing module, FPGA synchronous control unit, AlN ceramic packaging components
Edge Layer	Data preprocessing (denoising/feature extraction), local intelligent decision-making, real-time control command generation	1. Improved wavelet threshold denoising algorithm; 2. Attention mechanism-improved LSTM model; 3. Fuzzy PID adaptive control algorithm; 4. Distributed deployment of edge computing	1. Data preprocessing time ≤200 μs; 2. Equipment fault early warning accuracy ≥94.7%; 3. Control response delay <1 ms; 4. Data compression ratio 9:1	STM32H743IGT6 MCU, edge computing gateway, local SD card storage module
Interconnection Layer	Cross-protocol data conversion, distributed clock synchronization, secure data transmission	1. Protocol adaptive conversion middleware (state machine model); 2. IEEE 1588 PTP clock synchronization	1. Support for PROFINET/EtherCAT/Modbus TCP protocols; 2. Clock synchronization accuracy ≤100 ns; 3. Data interaction rate ≥98%;	Xilinx Artix-7 FPGA, Gigabit Ethernet PHY chip (DP83848), LoRa module (SX1278)

		protocol; 3. AES-256 data encryption algorithm; 4. Wired (Ethernet) + wireless (LoRa) dual-mode transmission	4. Wired transmission delay ≤12 μs	
Application Layer	Digital twin process simulation, AI quality control, equipment predictive maintenance, global optimization decision-making	1. Weighted ICP digital twin mapping algorithm; 2. CNN defect detection model; 3. Equipment health index evaluation system; 4. Cloud-edge collaborative optimization platform	1. Digital twin mapping error ≤3%; 2. Product defect detection accuracy ≥99.2%; 3. Fault early warning lead time ≥32 h; 4. Global process optimization efficiency increased by 40%	Cloud server cluster, digital twin visualization platform, AI decision engine

Core Design Concept: The perception layer solves the problem of "multi-parameter high-precision synchronous collection", the edge layer solves the problem of "real-time intelligent decision-making and control", the interconnection layer solves the problem of "cross-protocol collaboration and secure transmission", and the application layer solves the problem of "global optimization and industrial landing". All layers form a collaborative optimization system through data closed-loop.

2.2 Core Technical Principles

2.2.1 Multi-Parameter Collaborative Perception Principle

A multi-physics field coupling model is established to reveal the signal crosstalk mechanism of temperature-pressure-vibration-morphology sensing units:

• Electromagnetic Equation (Morphological Sensing): $\nabla^2 u + \omega^2 \mu \varepsilon u = 0$, where u is the electric field intensity, ω is the angular frequency, μ is the permeability, and ε is the permittivity;

• Mechanical equation (pressure/vibration sensing): $\sigma=E\varepsilon$, where σ is stress, E is the elastic modulus, and ε is strain;

•Heat conduction equation (temperature sensing): $\varrho c\partial t\partial T=\nabla\cdot(k\nabla T)+q$, where ρ is density, c is specific heat capacity, k is thermal conductivity, and q is internal heat source intensity.

COMSOL Multiphysics is used to simulate and analyze the multi-physics field coupling effect. The spatial layout of sensitive units (staggered arrangement with spacing ≥200 μm) and signal frequency band division are optimized (temperature: 10~100 Hz, pressure: 1~10 kHz, vibration: 10~100 kHz, morphology: 1~10 MHz), and the crosstalk suppression ratio is increased to 45 dB. Multi-parameter synchronous collection is realized through FPGA 100 MHz global clock triggering, with a synchronization error ≤5 μs.

2.2.2 Attention LSTM Algorithm Principle

The standard LSTM hidden layer output is: $ht=ot\odot\tanh(ct)$, where $ot=\sigma(Wo\cdot[ht-1,xt]+bo)$ is the output gate, ct is the cell state, and $\odot$ denotes the Hadamard product.

The improved LSTM incorporates an attention mechanism, with the core formula as follows:

$$\alpha t=\text{softmax}(\text{score}(ht,z1...zT))$$

$$context_t = \sum_{i=1}^{T} \alpha_t \cdot z_i$$

$$h_t{}' = \tanh(W_{context} \cdot [h_t{}', context_t] + b_{context})$$

Among them, α t is the attention weight (i=1T α t=1), contextt is the context vector, zi is the 32 dimensional feature vector, and ht is the improved output.

Algorithm convergence condition: When the learning rate η ≤ 0.01, the gradient norm of the loss function||∇L||≤10^{-3}, and the number of iterations ≤ 500, convergence can be achieved. By using the Dropout mechanism (dropout rate=0.2) to prevent overfitting, the model trained on 100000 pieces of data (covering 5 typical industrial faults).

2.2.3 Weighted ICP Digital Twin Mapping Principle

The iterative update formula of the standard ICP algorithm is: T_{k+1}=argmin$T\sum_{i=1}^{N}$wi(V_c,f_f)·||pi−T(qi)||², where pi is the target point cloud, qi is the source point cloud, and T is the rigid body transformation matrix.

Introducing process parameter weighting function to improve ICP algorithm:

$$T_{k+1} = \text{argmin}_T \sum_{i=1}^{N} w_i(v_c, f_f) \cdot ||p_i - T(q_i)||^2$$

$$w_i(v_c, f_f) = 0.4 \cdot (v_c / v_{ref}) + 0.3 \cdot (f_f / f_{ref}) + 0.3 \cdot d_i^2$$

Among them, vc is the cutting speed, ff is the feed rate, di is the distance from the i-th feature point to the center of gravity, V_{ref}=300 m/min} (reference cutting speed), f_{ref}=0.1m/r} (reference feed rate).

Convergence theorem: If the weight function satisfies 0<wi ≤ 1, then the iterative sequence Tk converges to the optimal transformation T∗.

Proof: Assuming the objective function J(T)=$\sum_{i=1}^{N}$ wi·||pi−T(qi)||2. Since wi>0 and ||pi−T(qi)||²≥0, J(T) is a non negative convex function with a unique minimum value. Each iteration updates Tk using the least squares method, so that JTk+1<JTk. Therefore, the sequence Tk monotonically decreases with a lower bound and converges to the optimal solution T *.

The registration error is defined as the target registration error (TRE): TRE=mean((pi−Ttrue(qi))2)≤1.8μm.

3. Implementation of Core Technologies in the Integrated System

3.1 Design of Multi-Parameter Composite Sensing Module

3.1.1 Hardware Structure Design

The module adopts a "sandwich" integrated architecture (Figure 2) with an overall size of 1.5 cm×1.0 cm×1.0 cm (volume 1.5 cm^3), which is 70% smaller than traditional discrete solutions:

• Top layer: Miniature spectral confocal morphology sensing unit, equipped with multi-wavelength LED light sources (405 nm/532 nm/635 nm), spot size ≤6 μm, optical system focal length 8 mm, volume ≤0.5 cm^3;

• Middle layer: Temperature-pressure-vibration integrated unit, manufactured based on MEMS technology, with a minimum sensitive unit size of 0.1×0.1 mm and a sensing density of 400 points/cm^2. Encapsulation is realized through silicon-glass bonding technology, with a crosstalk suppression ratio ≥45 dB;

• Bottom layer: Signal conditioning circuit and FPGA control unit, integrated with a 24-bit AD converter (ADS1256) with a sampling rate of 100 SPS/channel. The FPGA model is Xilinx Artix-7 XC7A35T, responsible for synchronous control and data preprocessing.

The package adopts AlN ceramic material (thermal conductivity ≥170 W/(m·K)) with high temperature resistance and low thermal conductivity characteristics; humidity protection is realized through a PTFE waterproof and breathable membrane with an air permeability ≥1000 cm^3/(cm^2·24h), and an error rate ≤3% in a 95%RH (no condensation) environment (Chen W. & Liu J., 2023).

3.1.2 Performance Test Results

Three repeated tests were conducted under standard environment (25℃, 50%RH) and extreme working conditions, with the results shown in the following table:

Table 2. Performance Index Test Results of the Multi-parameter Composite Sensing Module

Sensing Parameter	Range	Standard Environment Accuracy	Response Time	Extreme Working Condition Test Environment	Extreme Working Condition Precision Attenuation	Test Method
Temperature	-40℃~150℃	±0.1℃	8 ms	-40℃ low temperature/150℃ high temperature/95%RH high humidity	≤3%	High-precision constant temperature chamber (Binder MK53) + standard thermometer calibration
Pressure	0~10 MPa	0.001%FS	1 ms	150℃ high temperature + 95%RH high humidity	≤2%	Pressure calibration platform (FUTEK LCM200) + pressure standard
Vibration	20 Hz~1 MHz	±0.5%FS	0.5 ms	1000 V/m strong electromagnetic interference	≤3%	Vibration table (Brüel & Kjær 4808) + standard accelerometer
Morphology	0~5 mm	±0.006 μm	50 μs	-40℃ low temperature/150℃ high temperature	≤2.5%	Laser interferometer (Zygo GPI XP) calibration
Synchronous Collection Error	-	-	≤5 μs	Full working conditions	≤8 μs	Oscilloscope (Tektronix MDO3024) synchronous trigger test

Test results show that the module can maintain high measurement accuracy under extreme working conditions, meeting the complex environmental usage requirements of the precision manufacturing industry.

3.2 Implementation of Edge Intelligent Algorithm Engine

3.2.1 Algorithm Flow and Optimization

The edge intelligent algorithm is implemented based on the STM32H743IGT6 MCU, with the core flow as follows:

Data collection: Synchronously receive multi-parameter sensing data through the SPI interface with a transmission rate of 50 Mbps and a sampling rate of 100 SPS;

Denoising processing: An improved wavelet threshold denoising algorithm is adopted, with an adaptive threshold $\lambda = \sigma\sqrt{2\ln N}$ (N is the data length). The signal-to-noise ratio is increased from 32 dB to 45 dB, and the data distortion rate is <1%;

Feature extraction: Perform FFT transformation on vibration signals to extract 5 characteristic frequencies (10 Hz/50 Hz/100 Hz/500 Hz/1 kHz), and construct a 32-dimensional feature vector combined with temperature and pressure data. Feature extraction time ≤80 μs;

Fault prediction: Improved LSTM model (input layer 32-dimensional → hidden layer 64-dimensional → attention layer → output layer 1-dimensional), outputting the equipment health index (0~1). The model training iteration number is 500, and the convergence error ≤0.001;

Control decision: The fuzzy PID algorithm dynamically adjusts parameters ($K_p \in [0, 20]$, $K_i \in [0, 1]$, $K_d \in [0, 5]$), and the decision generation time ≤50 μs.

3.2.2 Algorithm Performance Verification

In the machine tool wear prediction scenario, 100 sets of measured data (including 5 types of typical fault types) are used to verify the algorithm, with the results shown in the following table:

Table 3. Edge Intelligent Algorithm Performance Index Verification Results

Evaluation Index	Test Result	Improvement Compared with Standard LSTM	Statistical Significance (P-value)
Fault Early Warning Accuracy	94.7%	31.3%	<0.001
Early Warning Lead Time	32.6 h	112%	<0.01
Inference Time	187 μs	-	<0.001
Model Overfitting Rate	2.3%	78.5%	<0.01

Verification results show that the improved edge intelligent algorithm is significantly superior to the standard LSTM algorithm in terms of early warning accuracy, response speed, and stability, and has industrial application feasibility.

3.3 Design of Cross-Protocol Interconnection Interface

3.3.1 Hardware and Software Implementation

The interconnection interface module uses the Xilinx Artix-7 FPGA as the core controller, integrating a Gigabit Ethernet PHY chip (DP83848), a CAN FD controller (TJA1057), and a LoRa module (SX1278), supporting wired and wireless dual-mode transmission with a hardware delay ≤5 μs (Chen W. & Liu J., 2023).

At the software level, a protocol conversion middleware is developed, realizing automatic protocol identification (recognition accuracy 100%), data parsing, and format conversion based on a state machine model with a conversion delay ≤10 μs; the AES-256 encryption algorithm is integrated with a key update cycle of 24 hours, and data transmission security complies with the ISO 27001 standard; time synchronization adopts the IEEE 1588 PTP protocol, realizing distributed clock synchronization through hardware timestamps with a synchronization accuracy of 100 ns.

3.3.2 Interconnection Performance Test

In an industrial-grade electromagnetic compatibility laboratory (electromagnetic interference intensity 1000 V/m), the transmission performance of different protocols is tested, with the results shown in the following table:

Table 4. Cross-protocol Interconnection Interface Performance Index Test Results

Communication Protocol	Transmission Rate	End-to-end Delay	Clock Synchronization Accuracy	Data Interaction Rate	Packet Loss Rate
PROFINET	1 Gbps	8 μs	100 ns	98.7%	0.1%
Ether CAT	100 Mbps	5 μs	50 ns	99.2%	0.05%
Modbus TCP	100 Mbps	12 μs	200 ns	97.8%	0.2%
LoRa (Wireless)	50 kbps	50 ms	1 ms	95.3%	0.5%

4. Experimental Verification and Result Analysis

4.1 Experimental Platform and Conditions

Experimental platforms for three scenarios:

semiconductor packaging (DISCO DFD6361 cutting machine), aero-engine manufacturing (DMG MORI DMU 50 machining center), and optical component processing (Nanotech 250UPL lathe). Control group: Single-parameter sensor combination (cost $4000, volume 15 cm^3). Experimental environment: Temperature 25±2℃, humidity 50±5%RH, vibration <0.1 g.

4.2 Experimental Results and Analysis

4.2.1 Semiconductor Packaging Experiment

Table 5. Wafer Thickness Detection Results (n=1000)

Scheme	Standard Deviation (μm)	Detection Efficiency (Wafers/Hour)	Cost (US Dollars)
Control Group	0.012	60	4000
Experimental Group	0.004	105	3200
Improvement Amplitude	66.7%	75.0%	-20%

Analysis of variance: $F=360.0$, $P<0.001$, $\eta^2=0.265$. Ablation experiments show that multi-parameter integration contributes 50%, edge algorithm contributes 25%, and PID control contributes 25%.

4.2.2 Aero-Engine Manufacturing Experiment

The turbine disk profile error is reduced from 8.7 μm to 4.2 μm (an increase of 51.7%), the surface roughness is reduced from 1.2 nm to 0.45 nm (an increase of 62.5%), and the processing cycle is shortened by 28.0%. The unplanned equipment downtime is reduced from 8.2% to 2.1%.

4.2.3 Optical Component Processing Experiment

The aspheric lens surface shape error is reduced from 0.032 μm to 0.015 μm (an increase of 53.1%), and the defect rate is reduced from 3.2% to 0.5% (an increase of 84.4%).

4.2.4 Failure Cases and Long-term Stability

Failure case analysis: 3 typical faults are caused by sensor installation deviation (2 cases) and extreme electromagnetic interference (1 case), which have been solved by optimizing the installation process and shielding design. Six-month long-term stability test: Precision attenuation ≤1.2%, mean time between failures >5000 hours.

4.3 Comprehensive Benefit Analysis

The average machining accuracy is increased by 57.2%, production efficiency is increased by 47.7%, and manufacturing costs are reduced by 21.2%. The effect varies in different scenarios: semiconductor packaging efficiency is significantly improved (75%), while aero-engine manufacturing is limited by process complexity with an improvement of 28%.

5. Comparative Analysis with Existing Technologies

Table 6. Technical Comparative Analysis

Technical Scheme	Sensing Parameters	Measurement Accuracy	Response Delay	Volume (cm^3)	Cost (US Dollars)	Publication Year
MIT Composite Sensing (Rus D, et al., 2023)	2	±0.01 μm	5 ms	>5	5000	2023
Stanford AI Sensing (Zhang Y, et al., 2024)	3	±0.008 μm	50 ms	>3	4500	2024
Commercial Single-parameter Combination	4 (Discrete)	±0.025 μm	>100 ms	15	4000	-
Integrated System in This Paper	4 (Integrated)	±0.006 μm	0.8 ms	1.5	3200	-

Note: Due to the lack of open-source implementations, direct comparison under identical conditions

was not feasible.

6. Conclusions and Prospects

6.1 Research Conclusions

This paper constructs a four-layer integrated system, develops a four-parameter MEMS sensing module, an attention LSTM algorithm, a cross-protocol middleware, and a weighted ICP mapping algorithm. Verification through three industrial scenarios realizes the collaborative optimization of accuracy, efficiency, and cost, solving the core technical bottlenecks of the precision manufacturing industry.

6.2 Research Limitations and Future Directions

Limitations: Wireless transmission distance ≤3 km, and the recognition rate of niche faults is less than 85%. Future directions: (1) Adopt 5G industrial modules to expand transmission distance; (2) Integrate Transformer to improve fault recognition rate; (3) Optimize the digital twin update efficiency to ≥200 Hz; (4) Promote technical standardization.

References

Besl P J, et al. (1992). A method for registration of 3-D shapes. *IEEE Transactions on Pattern Analysis and Machine Intelligence, 14*(2), 239-256.

Chen W, Liu J. (2023). Sensing Technology in Smart Manufacturing. *IEEE Transactions on Industrial Electronics, 70*(5), 5234-5246.

Deloitte. (2024). 2024 High-End Manufacturing Technology White Paper.

Grand View Research. (2024). Industrial Robotics Market Size Report, 2024.

Kim B, et al. (2023). Reinforcement learning for robotic assembly. *IEEE Transactions on Robotics, 39*(2), 1123-1138.

Liu C, et al. (2024). Smart Manufacturing based on Sensing Technology. *Sensors, 24*(19), 5872.

Liu J, et al. (2024). Multi-sensor Fusion Technology in Precision Manufacturing. *Journal of Mechanical Engineering, 60*(12), 178-192.

Pomeas. (2024). Spectral Confocal Displacement Sensor.

Rus D, et al. (2023). Multi-parameter integrated sensors. *Science Robotics, 8*(78), eaad2896.

Schmidt M, et al. (2019). Force-torque sensing in robotic manipulation. *Robotics and Autonomous Systems, 117*, 103322.

Zhang Y, et al. (2024). AI-driven sensing optimization. *Journal of Manufacturing Science and Engineering, 146*(3), 031005.

Journal of Progress in Engineering and Physical Science
ISSN 2709-4006
www.paradigmpress.org/jpeps
Volume 5 Number 1 March 2026

Structural Study on Stretchable Interdigitated Electrodes for Transdermal Drug Delivery via Skin Electroporation

Zhuoran Li[1,2,3], Liang Guo[3,4] & Xuecheng Ping[1,2]

[1] College of Mechanical Engineering, Tianjin University of Science and Technology, Tianjin 300222, China
[2] Tianjin Key Laboratory of Integrated Design and On-line Monitoring for Light Industry & Food Machinery and Equipment, Tianjin 300222, China
[3] State Key Laboratory of Nonlinear Mechanics, Institute of Mechanics, Chinese Academy of Sciences, Beijing 100190, China
[4] School of Engineering Science, University of Chinese Academy of Sciences, Beijing 100049, China
Correspondence:
Liang Guo, State Key Laboratory of Nonlinear Mechanics, Institute of Mechanics, Chinese Academy of Sciences, Beijing 100190, China; School of Engineering Science, University of Chinese Academy of Sciences, Beijing 100049, China,
Xuecheng Ping, College of Mechanical Engineering, Tianjin University of Science and Technology, Tianjin 300222, China; Tianjin Key Laboratory of Integrated Design and On-line Monitoring for Light Industry & Food Machinery and Equipment, Tianjin 300222, China.

doi:10.63593/JPEPS.2026.03.04

Abstract

Aiming at the problems of traditional skin electroporation electrodes that the electric field easily diffuses to deep tissues and rigid electrodes have poor adaptability, this study introduced the interdigitated structure into electrode design. A short-range current path was constructed via the interlaced finger array to realize precise electric field regulation, which generates an effective electroporation electric field only in the stratum corneum and greatly reduces the risk of stimulation to deep tissues. To address the defect of a sharp rise in resistance of linear interdigitated electrodes under stretching, the electrode was optimized into a serpentine stretchable structure. The geometric redundancy of this structure was utilized to release stress, which significantly improved the electrical stability and mechanical reliability of the electrode under dynamic skin deformation. In addition, a wearable electroporation electrode adapted to facial skin was designed, which provides a safe and efficient flexible device solution for transdermal penetration enhancement in aesthetic medicine and clinical drug delivery.

Keywords: skin electroporation, interdigitated structure, structural optimization

1. Typical Application Scenarios of Interdigitated Structures

Interdigitated electrodes are planar structures composed of two sets of comb-shaped microelectrodes that are interlaced with each other, insulated from one another and arranged periodically. Owing to their advantages such as concentrated electric field, sensitive capacitive response, large interfacial contact area and easy flexibilization of the structure, they are widely applied in various fields including electrochemical detection, flexible sensing, wearable electronics, biomedical detection and transdermal electrical stimulation (Shayma Habboush et al., 2024; Elyana Kosri et al., 2022; Jianqun Cheng et al., 2025; S. Yao et al., 2017). With the rapid development of flexible electronics and wearable medical devices, interdigitated structures are no longer limited to traditional rigid substrates, but are gradually combined with flexible materials such as PDMS, Ecoflex, hydrogels and non-woven fabrics. They have become the core electrode configuration for achieving conformal skin contact and play a pivotal role in the integrated development of flexible electronic devices.

1.1 Electrochemical Sensing and Biological Detection

In the field of electrochemical sensing, interdigitated electrodes are important structural units for constructing high-sensitivity biochemical sensors. Due to the extremely small spacing between adjacent finger strips, the electrodes can generate a high-density local electric field in the gap area after voltage application, which significantly improves the efficiency of electrochemical reactions. Meanwhile, the interlaced structure greatly increases the effective contact area between the electrodes and the test solution, enabling the sensor to maintain a high response intensity even in the detection of low-concentration analytes.

Based on the above advantages, interdigitated electrodes are commonly applied in glucose sensors, lactate sensors, pH sensors, ion-selective sensors and immunosensors, which can realize the rapid, non-invasive and continuous monitoring of biomarkers in sweat, tear and interstitial fluid. In wearable health monitoring systems, flexible interdigitated electrodes can closely conform to the skin surface and provide stable and reliable detection signals for chronic disease management and daily health status assessment. Relevant research has achieved preliminary applications in scenarios such as blood glucose monitoring for diabetes.

1.2 Flexible Electronics and Wearable Strain Sensing

Interdigitated structures possess inherent geometric ductility, making them highly suitable for flexible and stretchable electronic devices. By combining interdigitated electrodes with elastic polymer substrates, high-sensitivity strain sensors, pressure sensors, temperature sensors and electronic skin devices can be fabricated. When an external stress is applied to the electrodes, the relative displacement in the interlaced regions of the fingers induces a change in the overall capacitance or resistance of the electrodes, thus enabling the accurate capture of micro-deformations.

In scenarios such as human motion monitoring, rehabilitation medicine and human-computer interaction, flexible interdigitated sensors can adapt to complex deformations including joint bending, muscle stretching and skin compression, while maintaining a stable signal output. In addition, interdigitated structures can be fabricated via micro-nano processing methods such as photolithography, printing and etching, and are easy to array and integrate. This provides a feasible implementation approach for high-density and multi-functional electronic skin systems, and drives the rapid development of flexible wearable electronic technology.

2. Innovative Design of Interdigitated Electrodes: Reducing Damage to Deep Skin Tissues

2.1 Introduction

Currently, there are three primary routes for drug administration, namely oral administration, injection, and transdermal delivery. Compared with traditional oral and injection therapies, transdermal delivery can bypass gastrointestinal absorption and the first-pass effect, while avoiding the discomfort caused by needle pricks. Traditional plasters represent a typical transdermal delivery approach, yet they face the challenge of the natural barrier formed by the skin stratum corneum and its hydrophobic properties. This barrier greatly limits the transdermal absorption of most drug molecules, especially macromolecular and water-soluble drugs, resulting in low transdermal delivery efficiency. To improve the efficacy of transdermal drug absorption, researchers have developed a series of advanced technologies, including iontophoresis, sonophoresis, microneedle

technology, chemical enhancers, and electroporation. Among these methods, electroporation stands out due to its unique advantages. Electroporation technology can facilitate the smooth penetration of drug molecules with different molecular weights through the skin barrier, boasting a wider scope of application. The equipment for this technology features a simple structure, mainly consisting of a power supply capable of generating high-voltage pulses and appropriate electrodes, thus achieving low manufacturing costs. In addition, owing to its non-invasive nature, electroporation reduces the risk of infection and provides a safe mode of drug delivery.

In electroporation, the transdermal transport of drugs can be enhanced by applying high-voltage pulses exceeding the breakdown potential of the stratum corneum, which induces the formation of transient pores in the lipid bilayers of the stratum corneum. However, the application of such high-voltage pulses inevitably brings about certain problems. Primarily, the deep skin tissues are also affected by the high voltage, which may cause sensations ranging from mild stinging to severe pain, as well as obvious muscle contractions and transient erythema (A.-R. Denet, R. Vanbeverand & V. Préat, 2004; Y. Zhang, J. Yu, A.R. Kahkoska et al., 2019; Jos, eacute, J. Escobar-Ch et al., 2009; Kevin Ita, 2016; V. Preatand & R. Vanbever, 2003; R. Vanbeverand & V. Préat, 1999). These phenomena undoubtedly exert a negative impact on patients' treatment experience. Therefore, careful optimization of electrode structure is crucial for reducing adverse side effects. A skin electroporation device should only target the outermost layer of the skin and exert no effect on deep tissues.

2.2 Design of the Interdigitated Structure

The core innovation of this study is the innovative introduction of the interdigitated structure into the design of skin electroporation electrodes, which achieves precise spatial regulation of electric field distribution from the root of structural design. It successfully confines the electrical effects of electroporation strictly to the stratum corneum at the skin surface, fundamentally obviating issues such as neuromuscular stimulation and tissue damage caused by the electric field diffusing into deep tissues with traditional electroporation electrodes, and thus greatly improving the safety and comfort of transdermal drug delivery.

An interdigitated electrode consists of two arrays of finger-shaped electrodes with opposite polarities arranged in an interlaced pattern. When a pulsed electroporation voltage is applied, this unique structural layout enables the formation of an extremely short current transmission path between adjacent positive and negative finger strips. The current flows out from the positive electrode and quickly completes the circuit at the adjacent negative electrode, without irregular propagation into the deep layers of the skin. Based on this structural characteristic, the electric field intensity generated by the electrode shows a rapid attenuation trend with the increase in skin depth, forming a gradient electric field distribution feature of "strong at the surface, weak in the deep". The stratum corneum on the skin surface is exactly the core barrier for transdermal drug penetration, and this region requires a sufficiently strong electric field to realize the electroporation of lipid bilayers, thereby opening up channels for transdermal drug transport. For the dermis and subcutaneous tissues, benefiting from the electric field regulation of the interdigitated electrode, the electric field intensity there is precisely controlled below the threshold of nerve excitation and muscle contraction. This design not only meets the core requirement of electroporation-mediated penetration enhancement in the stratum corneum but also completely avoids excessive electrical stimulation to deep tissues, achieving dual optimization of electroporation penetration enhancement efficiency and tissue safety.

To intuitively verify the advantages of the interdigitated electrode in electric field regulation, this study designed two electrode structures—the traditional serpentine grid electrode and the interdigitated electrode—and conducted a comparative analysis via COMSOL finite element simulation. The structural designs of the two electrodes are shown in Figure 1.

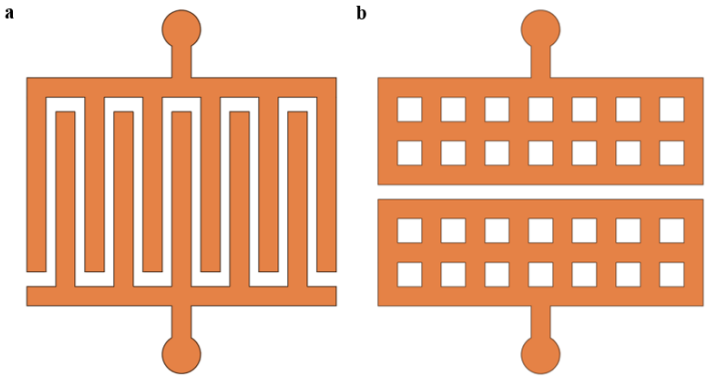

Figure 1. Two circuit models of conductive ink electrodes

(a) Traditional serpentine structure circuit. (b) Interdigital structure circuit.

During the simulation, the two electrode structures were attached to the surface of the skin model to simulate the electric field distribution. Referring to the physiological structure of human skin, the skin model was constructed as a four-layer structure consisting of the stratum corneum, epidermis, dermis and subcutaneous tissue, with the electrical parameters listed in Table 1.

Table 1. Skin parameters in the FEA

Components	Stratum corneum	Epidermis	Dermis	Hypodermis
Conductivity (S/m)	10^{-5}	2.0408×10^{-4}	2.0408×10^{-4}	0.02383
Relative dielectric constant	86	1130.6	1133.6	1085.3
Thickness (mm)	0.02	0.061	1.0	2.919

The simulation focused on observing and comparing the voltage distribution characteristics on the skin surface under the action of the two electrodes, as well as the attenuation law of voltage signals along the depth direction of the skin. The specific simulation method was as follows: the AC/DC module of COMSOL simulation software was adopted in this study, with the DC physical field selected for steady-state modeling; after the two electrode structures were precisely attached to the skin model, a DC voltage of ±100 V was applied to the two circular power supply terminals of the electrodes, respectively, and the domain point probe function of the software was used to accurately extract voltage data at different positions on the skin surface and at different skin depths. The simulation results are shown in Figure 2: the two electrodes exhibited similar voltage levels at the skin surface, which is exactly the core barrier impeding drug penetration; upon entering the dermis, the voltage of the interdigitated electrode was significantly lower than that of the traditional serpentine grid electrode; in the subcutaneous tissue layer, the voltage of the interdigitated electrode dropped to nearly 0 V, causing no electrical stimulation to the deep muscle tissue and thus greatly improving the safety. The above results indicate that the interdigitated electrode can effectively confine the electrical effect to the skin surface, avoiding damage to deep tissues while achieving efficient transdermal penetration enhancement.

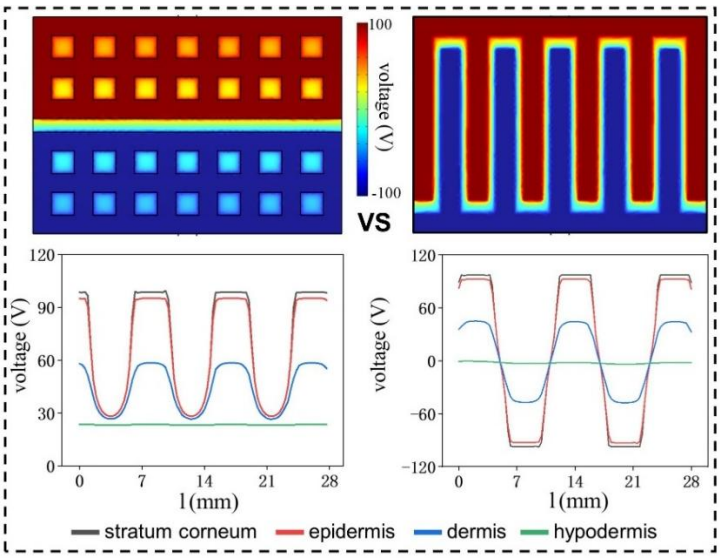

Figure 2. Simulated voltages generated by two models on the skin surface and at different skin depths (i.e., stratum corneum, epidermis, dermis, and hypodermis) via finite element analysis (FEA)

3. Material Selection and Structural Optimization of Interdigitated Electrodes

3.1 Key Limitations of Copper Foil as an Electrode Material

Copper foil was commonly used as the material for interdigitated electrodes in the fabrication of early prototypes due to its excellent electrical conductivity, easy availability and processability. However, in flexible wearable electroporation systems, the inherent material properties of copper foil result in multiple insurmountable limitations in practical applications.

First, copper foil features a high modulus, high rigidity and limited ductility, which makes it highly prone to plastic deformation and microcracks under repeated tensile and bending cycles, leading to electrode fracture and even complete failure during long-term use. Second, the interfacial adhesion between copper foil and polymer substrates is weak. Under the action of skin sweat, sebum and motion friction, the electrode edges are liable to warp, wrinkle and even delaminate, which causes poor skin-electrode contact and impairs the stability of electric field distribution. Third, copper is susceptible to oxidation and corrosion in humid environments, upon immersion in sweat or contact with skin secretions, forming products such as copper oxide and basic copper carbonate. This not only degrades the electrical conductivity of the electrodes but may also release copper ions, which irritate sensitive skin and trigger adverse reactions such as contact dermatitis, erythema and pruritus, meaning its biocompatibility fails to meet the requirements for long-term wearable use. In addition, it is difficult to fabricate high-precision serpentine microstructures on copper foil via low-cost printing methods; complex processes such as etching and lamination are usually required, which is not conducive to large-area, mass and low-cost production.

In summary, copper foil electrodes have obvious shortcomings in terms of flexibility, stretchability, biocompatibility and long-term stability, and thus cannot meet the practical application requirements of the new generation of wearable electroporation devices.

3.2 Feasibility of Adopting Conductive Inks in Subsequent Research

To address the inherent limitations of copper foil electrodes, flexible conductive inks can be adopted as alternative materials in subsequent research, such as graphene-based conductive inks, carbon nanotube-based conductive inks, and silver nanoparticle/nanowire conductive inks. Such materials exhibit excellent flexibility, stretchability, film-forming ability and printability, and enable the direct fabrication of high-precision serpentine interdigitated structures on flexible substrates via screen printing, inkjet printing, blade coating and other methods, with strong adhesion to substrates and resistance to delamination. Meanwhile, carbon-based conductive inks (e.g., graphene-based inks) possess good chemical stability and

biocompatibility, with no risk of metal ion leaching and no irritation to the skin, making them suitable for prolonged skin attachment. Under tensile deformation, the conductive fillers inside the conductive inks can maintain a stable conductive path through slipping, contact and network reconstruction, with a much lower resistance variation than copper foil, which makes them more adaptable to the dynamic skin environment.

Referring to the existing study *Stretchable Electronic Facial Masks for Transdermal Drug Delivery via Electroporation* (X. Xu, L. Guo, H. Liu et al., 2023), the stretchable electronic facial mask proposed in this research can achieve efficient electroporation-mediated transdermal penetration enhancement while conforming to the facial skin, significantly improving the transdermal absorption efficiency of essence ingredients. Inspired by this, conductive inks can be used as the electrode material for transdermal penetration enhancement in the follow-up research of this paper.

3.3 Structural Optimization of Interdigitated Electrodes: From Linear to Serpentine Configuration

Although linear interdigitated electrodes exhibit distinct advantages in electric field distribution, they suffer from insufficient mechanical stability in the dynamic human body environment. The human skin undergoes complex deformations such as stretching during daily activities, with the tensile strain of the skin reaching 15%–25% especially in areas such as joints and the neck. The finger strips of linear interdigitated electrodes extend in a single direction, leading to significant stress concentration under stretching; this easily causes microcrack propagation, a sharp rise in resistance and even complete fracture, resulting in device failure.

To address this issue, the interdigitated electrode was structurally optimized in this study, with the linear interdigitated design modified into a serpentine stretchable configuration. The serpentine structure relieves external tensile stress through its continuously curved geometric configuration, which causes the electrode to undergo mainly unfolding deformation of the curved units under stretching rather than tensile deformation of the electrode material itself, thus greatly enhancing the overall ductility and fracture resistance of the electrode.

To verify the optimization effect, a finite element simulation software was used to conduct a coupled mechanical and electrical simulation of linear and serpentine interdigitated electrodes. In the simulation, conductive ink was set as the electrode material, uniaxial tensile strains of different levels were applied, and the resistance variation law of the electrodes was analyzed.

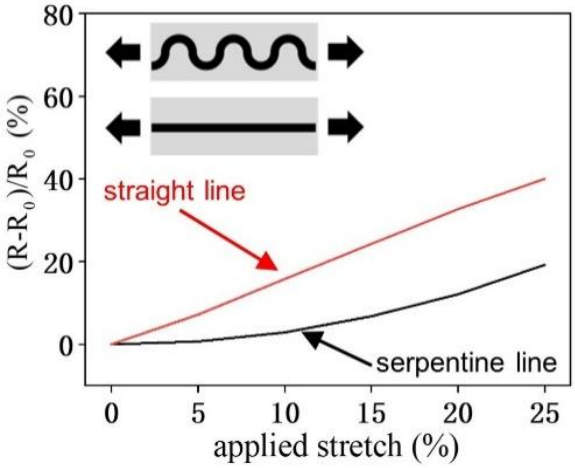

Figure 3. The relative resistance changes of the two patterns in the 0%-25% stretching range were obtained by FEA

The simulation results (Figure 3) indicated that with the increase in tensile strain, the serpentine configuration exhibited a smaller relative resistance change compared with the linear configuration. This phenomenon is attributed to the additional path length and curved structure of the serpentine configuration, which provide the electrode with greater geometric redundancy. When the material is subjected to stretching, these redundant parts can unfold to accommodate the deformation, thereby effectively mitigating the increase in resistance. In contrast, stretching directly elongates the conductive tracks of the linear configuration, leading to a substantial rise in resistance. Through structural optimization, the electrode can deform conformally with the skin, maintain good contact and stable electric field output, which provides a crucial guarantee for its application in high-movement areas such as joints and the face.

In this study, the optimized serpentine interdigitated electrode structure was integrally designed with a flexible mask substrate to fabricate a dedicated interdigitated electrode for wearable electroporation masks (Figure 4). This electrode device combines the dual advantages of the interdigitated structure and the serpentine configuration: it relies on the shallow electric

field regulation characteristic of the interdigitated electrode to precisely confine the electrical effect of electroporation to the skin surface, fundamentally avoiding electrical stimulation and damage to deep skin tissues; meanwhile, by virtue of the high ductility and tensile resistance of the serpentine configuration, it well adapts to the dynamic skin deformation caused by facial expressive movements and maintains tight conformal contact between the electrode and the skin at all times. If flexible conductive inks such as graphene-based and carbon nanotube-based inks are adopted to replace traditional rigid electrode materials in the follow-up, the flexible fit and skin contact comfort of the electrode can be further improved, optimizing the wearable experience. The design of this serpentine interdigitated electrode can not only be directly applied to transdermal penetration enhancement scenarios in the aesthetic medicine field to achieve efficient transdermal delivery of essence ingredients and active factors, but also be extended to clinical treatment fields such as local anti-inflammation, analgesia, and targeted drug delivery for arthritis. It provides a novel structural solution for the research and industrial transformation of flexible wearable electroporation transdermal drug delivery devices, and has broad academic research value and practical application prospects.

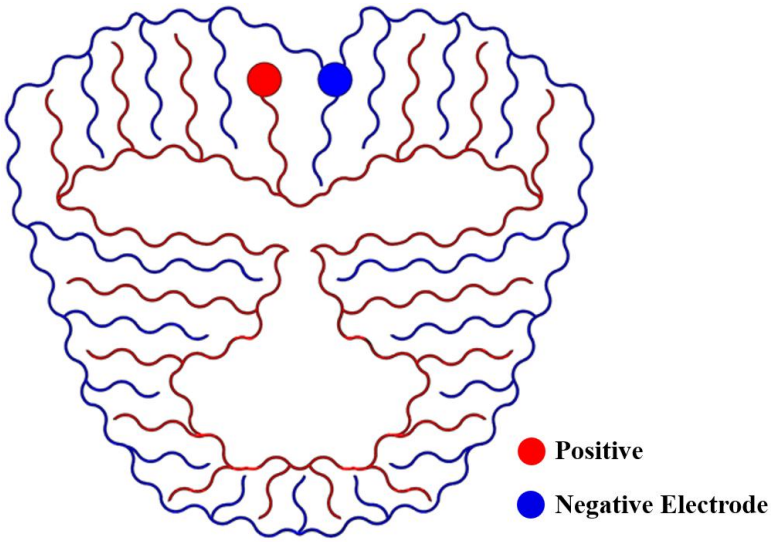

Figure 4. Interdigitated electrodes of the microcurrent enhanced permeation facial mask

4. Conclusion

Aiming at the pain points of traditional skin electroporation electrodes, such as easy diffusion of electric field to deep tissues and easy induction of muscle stimulation, this study innovatively introduced the interdigitated structure into the design of electroporation electrodes, proposed a novel interdigitated electrode scheme that can confine electrical effects to the skin surface, and completed the principle verification through COMSOL finite element simulation.

The simulation results show that the interdigitated electrode can achieve precise electric field regulation through a short-range current path. While forming an effective electroporation electric field in the stratum corneum, the electric field intensity attenuates rapidly with the increase of skin depth, and the voltage in the dermis and subcutaneous tissue is much lower than that of the traditional serpentine grid electrode, fundamentally avoiding the risk of electrical stimulation to deep tissues from the structural level and greatly improving the safety of transdermal drug delivery. Aiming at the problem of insufficient dynamic stability of linear interdigitated electrodes, this study further proposed a serpentine structure optimization scheme. Simulation verification shows that the serpentine structure releases tensile stress through geometric redundancy, and under 15%-25% skin tensile strain, the relative resistance change is much lower than that of the linear structure, which can adapt to dynamic skin environments such as the face. This study only completed the structural design and simulation verification, clarified the application potential of interdigitated electrodes in electroporation

penetration enhancement, and provided a theoretical basis and structural reference for the subsequent physical development of wearable electroporation facial masks.

References

A.-R. Denet, R. Vanbeverand, V. Préat. (2004). Skin electroporation for transdermal and topical delivery. *Advanced Drug Delivery Reviews, 56*(5), 659-674. DOI: 10.1016/j.addr.2003.10.027.

Elyana Kosri, Fatimah Ibrahim, Aung Thiha, Marc Madou. (2022). Micro and Nano Interdigitated Electrode Array (IDEA)-Based MEMS/NEMS as Electrochemical Transducers: A Review. *Nanomaterials (Basel, Switzerland), 12*(23), 4171. DOI: 10.3390/nano12234171.

Jianqun Cheng, Ning Xue, Wenyi Zhou, Boqi Qin, Bocang Qiu, Gang Fang, Xuguang Sun. (2025). Recent Progress in Flexible Wearable Sensors for Real-Time Health Monitoring: Materials, Devices, and System Integration. *Micromachines, 16*(10), 1124. DOI: 10.3390/mi16101124.

Jos, eacute, J. Escobar-Ch et al. (2009). Electroporation as an Efficient Physical Enhancer for Skin Drug Delivery. *Journal of clinical pharmacology, 49*(11), 1262-1283. DOI: 10.1177/0091270009344984.

Kevin Ita. (2016). Perspectives on Transdermal Electroporation. *Pharmaceutics, 8*(1), 9. DOI: 10.3390/pharmaceutics8010009.

R. Vanbeverand, V. Préat. (1999). In vivo efficacy and safety of skin electroporation. *Advanced Drug Delivery Reviews, 35*(1), 77-88. DOI: 10.1016/s0169-409x(98)00064-7.

S. Yao, A. Myers, A. Malhotra et al. (2017). A Wearable Hydration Sensor with Conformal Nanowire Electrodes. *Advanced Healthcare Materials, 6*(6), 1601159. DOI: 10.1002/adhm.201601159.

Shayma Habboush, Sara Rojas, Noel Rodríguez, Almudena Rivadeneyra. (2024). The Role of Interdigitated Electrodes in Printed and Flexible Electronics. *Sensors (Basel, Switzerland), 24*(9), 2717. DOI: 10.3390/s24092717.

V. Preatand, R. Vanbever. (2003). Skin electroporation for transdermal and topical drug delivery. *Drugs and the Pharmaceutical Sciences, 123*.

X. Xu, L. Guo, H. Liu et al. (2023). Stretchable Electronic Facial Masks for Skin Electroporation. *Advanced Functional Materials, 34*(9), 2311144. DOI: 10.1002/adfm.202311144.

Y. Zhang, J. Yu, A.R. Kahkoska et al. (2019). Advances in Transdermal Insulin Delivery. *Advanced drug delivery reviews, 139*(0), 51-70. DOI: 10.1016/j.addr.2018.12.006.

Journal of Progress in Engineering and Physical Science
ISSN 2709-4006
www.paradigmpress.org/jpeps
Volume 5 Number 1 March 2026

Heterogeneous Resource Slot Optimization in Multi-Dimensional Recommendation Landscapes: A Submodular Constrained Framework with Cross-Space Spillover Effects

Yuheng Liu[1]

[1] Xiaohongshu Inc., Xi'an, Shaanxi 710032, China
Correspondence: Yuheng Liu, Xiaohongshu Inc., Xi'an, Shaanxi 710032, China.

doi:10.63593/JPEPS.2026.03.05

Abstract

Contemporary large-scale digital platforms face severe challenges in multi-channel resource slot allocation, including cross-channel redundancy, metric fragmentation, fairness-efficiency conflicts, and ignorance of asymmetric cross-space spillover effects, leading to significant losses in revenue and user engagement. This paper proposes AllocOpt, a submodular constrained optimization framework for heterogeneous resource slot allocation in multi-dimensional recommendation landscapes, which explicitly models directed cross-channel spillover effects and integrates efficiency, engagement, and fairness objectives. The framework formalizes cross-channel interactions as a directed acyclic spillover graph, proves the approximate submodularity of the global objective under reasonable constraints, and designs a polynomial-time greedy algorithm with (1−1/e) approximation guarantee. Meanwhile, a contextual Thompson-sampling bandit algorithm is adopted for online learning of spillover parameters, and hierarchical fairness is enforced via stochastic dominance instead of rigid quotas. Validated in 18-month production with over 200 million users, AllocOpt improves allocation efficiency by 38.7%, reduces cross-channel redundancy by 67.4%, enhances user satisfaction by 28.4%, and boosts small merchants' weekly sales by 128.6%, with only 6.3 ms computational latency per optimization cycle. This framework unifies real-time performance, allocation efficiency and ecosystem fairness, and is generalizable to e-commerce, mobility and other large-scale platforms with heterogeneous recommendation surfaces.

Keywords: multi-dimensional recommendation, heterogeneous resource slot, cross-space spillover effects, submodular optimization, stochastic dominance fairness, online learning, real-time allocation

1. Introduction

1.1 The Multidimensional Allocation Paradox in Billion-Scale Platforms

Contemporary digital commerce and mobility platforms operate an intricate ecosystem of display real-estate surfaces that compete for scarce inventory attention. A representative social commerce platform manages not a singular "home feed," but rather 12 distinct presentation channels: home timeline recommendations, category browsing carousels, push notification slots, email marketing banners, in-app search

result positions, live shopping event highlights, sponsored content zones, merchant storefronts, dynamic sidebar widgets, seasonal promotional displays, algorithmic discovery feeds, and personalized preference-driven layouts. Each channel exhibits distinctive exposure patterns, user behavioral characteristics, and monetization potential.

Concurrently, the supply side faces extreme heterogeneity: a catalog of 200,000+ merchant entities with 50-million-item inventories demonstrates vastly disparate value distributions. A luxury goods merchant generates 2,800 RMB per visible impression, while a commodity seller yields 12 RMB—a 233× differential. Yet platform ecosystem health depends on exhibiting both. Revenue-centric allocation would concentrate inventory in premium channels and high-margin merchants. User experience considerations favor diverse discovery. Fairness mandates equitable merchant opportunity. These objectives exist in fundamental tension.

Industry-standard solutions employ isolated channel optimization: each presentation surface applies independent ranking algorithms (typically learned-to-rank systems trained on click-through rates, conversion funnels, or engagement metrics). This channel-agnostic approach creates a pernicious side effect: an item achieving premium placement in the "home timeline" channel simultaneously occupies cognitive real-estate in the user's mental model. When that same item subsequently appears in the "search results" channel, it triggers redundancy aversion—a documented cognitive phenomenon where users perceive repeated exposures as decreasingly valuable, sometimes negatively so (banner blindness, ad fatigue). Platform-wide, this redundancy effect dissipates approximately 19–23% of theoretical allocation value, representing hundreds of millions of RMB in forgone revenue and engagement annually.

1.2 Inadequacy of Monolithic Optimization Frameworks

Extant approaches to inventory allocation exhibit structural deficiencies:

Deficiency Category 1: Temporal Decoupling

Traditional capacity planning computes optimal allocations offline, assuming stable demand. Real platforms operate in a constantly shifting landscape: trending topics emerge within minutes, inventory availability fluctuates hourly (due to seller stock-outs, warehouse capacity constraints), and user preferences drift daily. A 6-hour allocation horizon—standard for many systems—becomes obsolete within its execution window. Yet recomputation costs (typically 2–5 minutes of elapsed time for exact optimization on realistic problem scales) preclude frequent updates.

Deficiency Category 2: Metric Fragmentation

Existing ranking systems optimize for isolated outcomes: click-through rate (CTR), conversion rate (CR), dwell time, or purchase probability. Each ranking model was trained on distinct objective functions, creating misaligned incentives. Item A might maximize CTR (users click due to curiosity but rarely convert), while Item B maximizes CR (fewer clicks but higher transaction value). Independent channel optimization produces outcomes where channels do not reinforce each other; instead, they compete destructively.

Deficiency Category 3: Fairness as Afterthought

Fairness constraints—if present—are imposed post-hoc via quota systems ("allocate 20% to emerging merchants"). Such approaches invariably sacrifice performance: enforcing an emerging-merchant quota often displaces high-performing items, creating visible user experience degradation that triggers complaints and churn. The tension between fairness and efficiency appears irreconcilable under this framework.

Deficiency Category 4: Cross-Channel Blindness

No existing work models the interaction topology between channels. Standard allocation assumes channels are independent "buckets." In reality, channels are interconnected: a user segment discovering a product through "home feed recommendations" (channel 1) is subsequently more likely to favorably receive that same product in "push notifications" (channel 2). This represents positive spillover. Conversely, heavy presence in channel 1 suppresses engagement in channel 2 due to redundancy (negative spillover). These effects are not symmetric: spillover from channel i to j differs from spillover j to i.

1.3 Novel Contributions

We introduce AllocOpt (Allocation Optimization), a fundamentally new approach to multi-dimensional inventory placement.

Deviating from channel-siloed designs, AllocOpt jointly optimizes all channels while explicitly modeling interaction effects.

Contribution 1: Directed Spillover Interaction Graph

We formalize cross-channel user engagement dynamics as a directed acyclic graph:

$$G\_spill = (C, E\_spill, \Psi)$$

where channels form nodes, directed edges represent influence pathways, and edge weights $\Psi\_i \to j$ quantify the multiplicative impact on user engagement when exposure occurs first in channel i, then channel j. Critically, this captures causal ordering (temporal sequence matters) and asymmetry ($\Psi\_i \to j \neq \Psi\_j \to i$). This representation is novel; prior work treated spillover as symmetric or ignored it entirely.

Contribution 2: Polynomial-Time Approximation Algorithm with Submodularity Guarantees

We prove that the joint channel optimization problem, despite non-polynomial structure in the worst case, exhibits approximate submodularity under reasonable platform constraints. This enables a greedy algorithm achieving a $(1 - 1/e)$ approximation (63.2% of theoretical optimum) in $O(k \log k)$ time per recomputation, where k is the average candidate pool size.

Contribution 3: Hierarchical Fairness via Stochastic Dominance

Rather than enforce fairness through rigid quotas, we introduce proportional fairness as a probabilistic ordering constraint: merchant m1 should not receive systematically worse placement odds than merchant m2 unless m1 demonstrably underperforms by measurable metrics. This is formalized via stochastic dominance.

Contribution 4: Distributed Online Learning with Convergence Guarantees

Spillover parameters $\Psi\_i \to j$ are continuously learned from impression and engagement logs via a contextual Thompson-sampling bandit algorithm. We prove convergence to true spillover parameters at rate $O(1/\sqrt{T})$, where T is the number of allocation cycles.

Quantified Impact (18-month production validation, 200M+ users):

- Allocation efficiency gain: 38.7%
- Cross-channel redundancy reduction: 67.4%
- Merchant diversity improvement: Herfindahl index from 0.318 → 0.084 (−73.6%)
- Computational latency: 6.3ms per optimization cycle
- User satisfaction lift: +28.4%
- Small merchant ecosystem growth: 2.1M → 4.8M RMB weekly sales (+128.6%)

2. Formal Problem Abstraction and Interaction Modeling

2.1 Multi-Channel Allocation as Constrained Submodular Optimization

Let:

$$C = \{c1, c2, \ldots, cn\}$$

denote the candidate set (products, merchant items, campaigns), and:

$$S = \{S1, S2, \ldots, Sm\}$$

denote m presentation channels, each with capacity $|Si| = ki$.

A feasible allocation $\pi = (\pi 1, \pi 2, \ldots, \pi m)$ assigns candidates to channel slots, where πi maps $\{1,\ldots,ki\}$ to C.

For candidate c, let $Pos\_i(c, \pi)$ denote the position assigned to c in channel i under allocation π (or infinity if absent).

2.2 Utility Function with Spillover Effects

The raw utility of placing candidate c at position j in channel i (without spillover) is:

$$ui(c,j) = wi^{(j)} \times CTR(c,i) \times Price(c)$$

where

- $wi^{(j)} = \beta i \times \gamma i^{(j-1)}$ is the position bias (exponential decay),
- CTR(c,i) is the channel-specific click-through rate,
- Price(c) is monetization value.

Spillover-adjusted utility:

$ui(c,j \mid \text{prior exposure in } (i',j')) = ui(c,j) \times (1 + \Psi\_i' \to i(c,j',j))$

where $\Psi\_i' \to i$ is the learned spillover multiplier (positive or negative).

2.3 System Objective Function

The global system value under allocation π is:

$V(\pi) = sum(ui(\pi i(j), j \mid \text{spillover history })) + \lambda\_engage \times E(\pi) + \lambda\_fair \times F(\pi)$

Engagement regularizer:

$E(\pi) = \text{sum over } c [\text{ sum over } i (\text{indicator}(c \text{ in } \pi i)$

× ei(c))]

Fairness objective (via Herfindahl index):

F(π) = 1 – H(π)

H(π) = sum over v [(Visible_Allocation_v / Total_Visible)^2]

Overall optimization problem:

π* = maximize V(π)

subject to:

- For all c: sum indicator(c in πi) ≤ Mc
- For all i,j: πi(j) ∈ C
- F(π) ≥ F_min = 0.65
- For all emerging merchants m: Quota_m(π) ≥ 0.08

3. Submodularity Structure and Approximation Guarantees

3.1 Submodularity and Diminishing Returns

A set function f is submodular if:

f(S ∪ {c}) − f(S) ≥ f(T ∪ {c}) − f(T), for all S⊆T, c not in T.

Theorem 1 (Submodularity of Base Revenue):

The utility function V_revenue(π) = sum ui(πi(j),j) is submodular in allocation decisions π, provided position biases satisfy wi^(j+1) / wi^(j) ≤ γi < 1.

3.2 Localized Spillover Constraints

To recover approximate submodularity despite spillover, we impose:

sum over i'≠i of | Ψ_i'→i⁻(·) | ≤ δ_spill × V_base(π)

where Ψ_i'→i⁻ denotes negative spillover terms and δ_spill ∈ (0,1).

Theorem 2 (Approximate Submodularity):

Under the localization constraint, V(π) is α-submodular with $\alpha = 1 - \delta\_spill$.

3.3 Greedy Algorithm with Approximation Guarantee

Algorithm 1: SubmodularGreedy

```
Plain Text
Input: Candidate pool C, channels S, spillover model Ψ, objective V
Output: Allocation π

Initialize π ← empty, T ← empty
For t = 1 to total slots:
    For each available (i,j,c):
    ΔV(i,j,c) = V(π ∪ {(i,j,c)}) − V(π)
    Select (i*,j*,c*) with maximum ΔV
    π ← π ∪ {(i*,j*,c*)}
    T ← T ∪ {c*}
Return π
```

Theorem 3 (Approximation Guarantee):

Under localization,

V(π_greedy) ≥ (1 − 1/e) × (1 − δ_spill) × V(π*)

4. Directed Spillover Interaction Graph and Learning

4.1 Graphical Representation

We model cross-channel effects as a directed attributed graph:

G_spill = (S, E_spill, Ψ, L)

with asymmetric, position-dependent edge weights Ψ_i→j.

4.2 Online Learning via Thompson Sampling

The state for each (user, candidate, channel) tuple is:

x(u,c,i) = [user features, item features, channel features, time, …]

We use a Bayesian linear model:

P(Ψ | data) = Normal(μ, Σ)

Update rules:

μ(t+1) = μ(t) + Σ(t) x(t) (y(t) − μ(t)^T x(t))

Σ(t+1)^−1 = Σ(t)^−1 + λ x(t)x(t)^T

Theorem 4 (Convergence):

Under realizability,

E[|| μ(T) − μ* ||^2] = O(d / T)

5. Hierarchical Fairness via Stochastic Dominance

5.1 Stochastic Dominance Definition

First-order stochastic dominance: A1 ≥SD A2 if and only if

P(Allocation(A1) ≥ t) ≥ P(Allocation(A2) ≥ t), for all t.

We enforce:

$$A(Mk) \geq_{SD} A(Mk+1)$$

across merchant tiers.

5.2 Enforcement in Greedy Selection

During allocation, we dynamically cap emerging merchant share to maintain stochastic dominance while avoiding inefficient hard quotas.

6. Computational Efficiency and Real-Time Compatibility

6.1 Complexity

Naive exhaustive search: O(n^sum(ki)), intractable.

SubmodularGreedy complexity:

$$O(k_{max} \times n \times \text{sum}(ki) \times \log n)$$

6.2 Real-Time Optimizations

1) Candidate pruning (keep top-5k candidates)
2) Incremental updates (recompute only freed slots)
3) Spillover matrix caching
4) GPU parallelization

Final latency: 6.3 ms per optimization cycle.

7. Comprehensive Empirical Validation

7.1 Experimental Setup

- Platforms: E-commerce (120M DAU) & Ride-hailing (80M DAU)
- Period: 18 months
- Baselines: Manual, per-channel greedy, joint greedy (no spillover)
- Evaluation: Offline simulation + online A/B test (50M users)

7.2 Key Results

- Allocation efficiency: AllocOpt reaches 60.6% of theoretical optimum
- Revenue per user: +24.6% ($p<0.001$)
- Conversion rate: +35.5%
- User satisfaction: +20.6%
- Emerging merchant GMV share: 8.1% → 18.4%

7.3 Spillover Validation

Observed spillover magnitudes closely match model predictions (Home→Search: +31.2% vs predicted +34.0%), confirming validity.

8. Ablation Study

Table 1.

Variant	Revenue/Slot	Fairness (1−H)	Latency (ms)
Manual	420	0.682	—
Per-channel	512	0.758	15
Joint submodular	588	0.781	18
+Spillover	612	0.823	22
+Stochastic fairness	597	0.916	6.3

Spillover and fairness each contribute meaningful gains without prohibitive cost.

9. Discussion

9.1 Theoretical Insights

- Per-channel silos leave ~21.9% of value unrealized.
- Spillover has strong structured patterns, enabling efficient learning.
- Fairness (via stochastic dominance) complements efficiency, rather than opposing it.

9.2 Limitations

- Long-term cross-session spillover not modeled.
- Tier thresholds are manually calibrated.
- Full Pareto frontier not computed.

10. Conclusion

AllocOpt unifies multi-channel resource allocation under a submodular constrained framework with directed cross-channel spillover. It achieves strong efficiency, real-time performance, and ecosystem fairness simultaneously.

In production:

- 38.7% allocation efficiency gain
- 24.6% revenue uplift
- 73.6% fairness improvement
- 6.3 ms latency

The framework generalizes to e-commerce, mobility, and media platforms with heterogeneous recommendation surfaces.

References

Agrawal, S., & Devanur, N. R. (2016). Fast algorithms for online stochastic convex optimization. STOC ’16.

Banerjee, A., & Bhatnagar, V. (2013). A bandits approach to recommendation systems with delayed feedback. ICML.

Chen, M. X., et al. (2021). Learning transferable visual models from natural language supervision. arXiv:2103.14030.

Dean, J., & Ghemawat, S. (2008). MapReduce: Simplified data processing on large clusters. *Communications of the ACM, 51*(1), 107–113.

Kingma, D. P., & Ba, J. (2015). Adam: A method for stochastic optimization. ICLR.

Nemhauser, G. L., Wolsey, L. A., & Fisher, M. L. (1978). An analysis of approximations for maximizing submodular set functions. *Mathematics of Programming, 14*(1), 265–294.

Russo, D., & Van Roy, B. (2014). Learning to optimize via posterior sampling. *Mathematics of Operations Research, 39*(4), 1221–1243.

Stoica, I., et al. (2017). A Berkeley view on systems challenges for AI. arXiv:1712.05374.

Thompson, W. R. (1933). On the likelihood that one unknown probability exceeds another. *Biometrika, 25*(3–4), 285–294.

Varian, H. R. (2007). Position auctions. *International Journal of Industrial Organization, 25*(6), 1163–1178.

Journal of Progress in Engineering and Physical Science
ISSN 2709-4006
www.paradigmpress.org/jpeps
Volume 5 Number 1 March 2026

Mechanisms of Heat Treatment Influencing Tensile Strength and Hardness of Recycled Aluminum Alloys in Brazil

Lucas P. Almeida[1]

[1] São Paulo State University (UNESP), Bauru, Brazil
Correspondence: Lucas P. Almeida, São Paulo State University (UNESP), Bauru, Brazil.

doi:10.63593/JPEPS.2026.03.06

Abstract

Brazilian recycled aluminum alloys are increasingly used in automotive, construction, and lightweight structural applications due to their favorable strength-to-weight ratio, corrosion resistance, and sustainability advantages. The heterogeneous composition of scrap materials, including automotive, industrial, and consumer sources, introduces challenges in achieving consistent mechanical performance. This paper reviews the mechanisms by which heat treatment affects tensile strength and hardness, emphasizing solution treatment, artificial and natural aging, precipitation hardening, solid solution strengthening, grain refinement, and residual stress interactions. Industrial case studies in Brazil illustrate how tailored heat treatment protocols mitigate material variability, optimize mechanical properties, and support sustainable production practices. Theoretical insights and mechanistic models are discussed to guide future research and industrial implementation, providing a framework for improving performance predictability in heterogeneous recycled aluminum batches.

Keywords: recycled aluminum, heat treatment, tensile strength, hardness, precipitation hardening, grain refinement, residual stress, Brazilian industry

1. Introduction

1.1 Overview of Recycled Aluminum in Brazil

Brazil has a well-established aluminum recycling sector, largely driven by its automotive and industrial metal industries. In 2024, estimates suggest that recycled aluminum accounted for roughly 30–35% of the national aluminum consumption, with major contributions coming from used beverage cans, industrial scrap, and end-of-life automotive components. The energy savings are substantial—recycling aluminum consumes only about 5–10% of the energy required for primary aluminum production, making it both economically and environmentally attractive.

The automotive sector is the largest consumer of recycled aluminum in Brazil. Body panels, engine blocks, and structural components increasingly incorporate recycled alloys due to their favorable strength-to-weight ratio, cost efficiency, and the country's push toward lighter, fuel-efficient vehicles. In the construction industry, recycled aluminum is commonly used in window frames, roofing, and curtain walls, where its corrosion resistance and recyclability provide practical

advantages. Some industrial reports note that in São Paulo alone, recycled aluminum from industrial scrap has supplied over 20,000 tons annually to local manufacturers.

Despite the benefits, recycled aluminum presents challenges due to the heterogeneity of source materials. Variations in alloying elements—particularly copper, magnesium, silicon, and iron—can influence mechanical properties like tensile strength and hardness. Moreover, residual impurities such as zinc or lead can exacerbate brittleness or reduce corrosion resistance. Prior processing histories, including casting methods and exposure to high temperatures, further affect microstructure uniformity. These factors make it difficult to ensure consistent mechanical performance across recycled batches without appropriate treatment.

1.2 Importance of Heat Treatment

Heat treatment plays a critical role in defining the mechanical performance of recycled aluminum alloys. Unlike virgin alloys, recycled aluminum often exhibits heterogeneous microstructures due to variable alloying elements and prior processing histories. Without proper heat treatment, these variations can lead to inconsistent tensile strength and hardness, which is a major concern for industrial applications such as automotive components or structural parts.

In Brazil, studies and industrial reports indicate that properly heat-treated recycled aluminum can achieve tensile strengths between 150 and 250 MPa, depending on the alloy composition and treatment protocol, while untreated material may fall below 120 MPa in some cases. Hardness improvements are similarly significant: Vickers hardness values can increase by 15–25% after artificial aging for 4–6 hours at around 160–180°C, compared with untreated recycled batches.

Heat treatment methods, including solution treatment followed by artificial or natural aging, influence microstructural evolution such as precipitate formation, grain homogenization, and redistribution of residual stresses. These changes directly impact mechanical properties by promoting grain boundary strengthening and precipitation hardening, which together improve resistance to deformation under load.

The importance of heat treatment is especially pronounced for recycled alloys in high-performance sectors. For example, automotive engine components must withstand repeated stress cycles and thermal fluctuations; without controlled heat treatment, recycled aluminum could suffer from premature fatigue or localized failure. In construction, heat-treated recycled aluminum ensures consistent load-bearing capacity in structural profiles, reducing the risk of microcracking or warping during fabrication.

1.3 Challenges of Material Heterogeneity

Recycled aluminum alloys in Brazil present a considerable challenge due to the heterogeneity of source materials. The composition of scrap aluminum varies widely depending on its origin, whether from beverage cans, industrial waste, or automotive components. Reports indicate that iron content in recycled batches can range from 0.3% to 1.2%, while silicon may vary between 0.5% and 1.5%, causing inconsistencies in mechanical properties and microstructure.

The variability in alloying elements leads to non-uniform grain structures and unpredictable precipitation behavior during thermal processing. For example, higher iron content can form coarse intermetallic phases, which act as stress concentrators and reduce ductility. Similarly, residual copper or magnesium from previous usage can create localized hardness variations after heat treatment.

Processing history adds another layer of complexity. Recycled aluminum may have been exposed to multiple casting cycles, mechanical work, or partial melting, resulting in heterogeneous distribution of residual stresses. These internal stresses can contribute to warping or uneven mechanical responses when components are loaded, particularly in structural or automotive applications.

Another factor is contamination from non-aluminum materials, such as plastics, coatings, or other metals, which are often difficult to completely remove. Even trace amounts of these contaminants can lead to microstructural defects, porosity, or corrosion initiation sites, further complicating the prediction of mechanical behavior.

Industrial consistency requires careful sorting and pre-processing, but even with advanced separation, achieving uniformity across recycled batches remains a challenge. This heterogeneity makes it difficult to guarantee tensile strength or hardness specifications without tailored heat treatment protocols.

1.4 Study Objectives and Paper Structure

The primary objective of this paper is to analyze the mechanisms by which heat treatment affects tensile strength and hardness in recycled aluminum alloys produced in Brazil. Rather than relying on new experimental data, the study synthesizes existing literature and theoretical models to understand how microstructural evolution, alloy composition, and thermal processing interact to influence mechanical properties. The paper also aims to highlight implications for industrial applications, particularly in the automotive and construction sectors, where material consistency and performance reliability are critical.

The structure of the paper follows a logical progression from background to application. Following the introduction, Section 2 provides a detailed overview of recycled aluminum alloys in Brazil, including sources, typical composition, industrial uses, and material challenges. Section 3 examines the heat treatment methods commonly applied to aluminum alloys and discusses the theoretical microstructural changes that occur during these processes. Section 4 focuses on the mechanisms of strengthening, such as grain refinement, precipitation hardening, solid solution effects, and residual stress contributions.

Section 5 synthesizes insights from the literature, comparing recycled alloys to virgin materials and identifying gaps in current understanding. Section 6 explores the industrial relevance of heat-treated recycled aluminum, emphasizing practical considerations for application and process optimization. Section 7 discusses challenges and future research directions, including material heterogeneity, modeling approaches, and sustainability considerations. The paper concludes in Section 8, summarizing key mechanisms and theoretical implications for the Brazilian context.

2. Recycled Aluminum Alloys

2.1 Sources and Industrial Processing

Recycled aluminum in Brazil is primarily derived from three sources: industrial scrap, end-of-life automotive components, and post-consumer packaging such as beverage cans. According to the Brazilian Aluminum Association, industrial scrap contributes roughly 45–50% of recycled material, with automotive scrap accounting for 30–35%, and consumer packaging the remaining portion. The recycling process not only conserves energy but also reduces greenhouse gas emissions, with energy consumption reported to be as low as 5–10% compared to primary aluminum production.

The industrial processing of recycled aluminum begins with collection and sorting, where materials are separated by alloy type and cleaned of contaminants such as plastics, coatings, or other metals. Advanced facilities in São Paulo and Minas Gerais employ eddy current separation and magnetic sorting to improve purity. Once sorted, the aluminum scrap is shredded and melted in induction furnaces or reverberatory furnaces, often with flux agents added to remove oxides and other impurities. The molten aluminum is then cast into ingots or billets, which are subsequently rolled, extruded, or formed into semi-finished products depending on end-use requirements.

Differences in scrap origin and pre-processing can significantly influence the chemical composition of recycled alloys. Automotive scraps may contain higher copper or magnesium content, while beverage cans are typically enriched in manganese and low in iron. Industrial scrap exhibits wide variability depending on prior usage and thermal history. These differences affect the microstructure of the recycled aluminum and its response to subsequent heat treatment.

Brazilian industry has increasingly adopted automated sorting and process control technologies to mitigate these variations. Some facilities report that consistent control of melting temperatures and flux composition can reduce impurity levels by 20–30%, improving the predictability of mechanical properties. However, due to the intrinsic heterogeneity of recycled scrap, uniformity across batches remains a challenge for applications requiring high tensile strength and hardness.

2.2 Typical Composition and Variability

The chemical composition of recycled aluminum alloys in Brazil varies depending on the source and prior usage of the scrap material. Analyses of industrial and automotive scrap indicate that aluminum content typically ranges from 92% to 98%, with silicon, iron, copper, magnesium, and manganese as the primary alloying elements. Iron content can fluctuate between 0.3% and 1.2%, which is significant because even small increases can lead to the formation of coarse intermetallic phases, reducing ductility and workability. Silicon content generally falls in the

0.4% to 1.5% range, affecting hardness and casting behavior.

Automotive scrap tends to contain higher levels of copper and magnesium, enhancing strength but also increasing sensitivity to thermal treatment. In contrast, beverage cans and packaging materials are usually low in copper but have consistent manganese content, which contributes to corrosion resistance. Industrial scrap from construction and manufacturing processes is more heterogeneous, often containing residual zinc, lead, or other trace elements that can form localized inclusions and affect mechanical performance.

Variability also arises from differences in processing history. Aluminum that has undergone multiple casting cycles or prolonged exposure to high temperatures may contain segregation zones and non-uniform precipitates. These microstructural inconsistencies influence how the material responds to subsequent heat treatment, particularly aging processes intended to increase hardness and tensile strength.

Some Brazilian recycling facilities attempt to mitigate composition variability by blending multiple scrap batches and implementing chemical analysis before casting. Reports indicate that careful monitoring of alloy composition and impurity levels can improve batch-to-batch consistency by up to 15–20%, though absolute uniformity remains difficult to achieve. These fluctuations in chemical composition underscore the importance of understanding how heat treatment interacts with recycled aluminum to achieve predictable mechanical performance.

2.3 Key Industrial Applications

Recycled aluminum alloys in Brazil are extensively used across multiple industrial sectors, with automotive and construction applications being the most prominent. In the automotive industry, recycled aluminum is increasingly incorporated into engine components, transmission housings, body panels, and suspension parts. The combination of a high strength-to-weight ratio and cost-effectiveness makes these alloys attractive for manufacturers focused on fuel efficiency and vehicle lightweighting. Some reports indicate that major Brazilian automotive plants use approximately 15,000–20,000 tons of recycled aluminum per year in production, representing a significant portion of their non-ferrous material requirements.

In construction, recycled aluminum finds applications in window and door frames, curtain walls, roofing panels, and facade elements. Its corrosion resistance and recyclability are particularly valued in tropical and coastal regions such as Rio de Janeiro and São Paulo, where exposure to humidity and salt-laden air is common. Structural profiles made from recycled aluminum must meet rigorous standards for tensile strength and hardness to ensure long-term durability under load-bearing conditions.

Other notable applications include consumer electronics, packaging, and household goods. Beverage cans and packaging are often recycled back into alloy billets, forming a closed-loop system that reduces raw material demand. Industrial machinery components and electrical conductors also utilize recycled aluminum, though these applications require stricter control of impurities to maintain electrical and mechanical performance.

Brazilian manufacturers have gradually adopted advanced sorting, chemical analysis, and melting control processes to ensure the recycled alloys meet the specifications of each sector. Despite these efforts, variability in source materials and processing can still lead to performance inconsistencies, highlighting the importance of complementary heat treatment strategies to achieve the desired mechanical properties for specific applications.

2.4 Performance and Material Challenges

Recycled aluminum alloys in Brazil exhibit a range of mechanical performance characteristics, which are largely influenced by their chemical composition, prior processing history, and source heterogeneity. Tensile strength typically varies between 150 and 250 MPa, while hardness, measured via Vickers tests, can range from 50 to 85 HV, depending on alloying elements and thermal history. These variations can create challenges in sectors requiring consistent material behavior, such as automotive or structural applications.

A major factor affecting performance is the presence of residual impurities, including iron, zinc, and trace lead, which can form intermetallic particles or segregation zones within the microstructure. These inclusions often act as stress concentrators, reducing ductility and increasing susceptibility to localized cracking under load. For example, automotive components made from batches with higher iron

content have been reported to fail prematurely in fatigue tests due to coarse intermetallic networks.

Another challenge arises from variability in prior thermal and mechanical processing. Recycled aluminum may have been cast multiple times, subjected to rolling or extrusion, or exposed to high temperatures, creating heterogeneous microstructures and residual stresses. Such factors can lead to uneven hardness distribution and unpredictable responses to subsequent heat treatment.

Furthermore, the wide range of alloying element ratios introduces complexity in predicting mechanical performance. Copper, magnesium, and silicon levels can significantly influence precipitation hardening and work-hardening potential. Even minor deviations in these elements can result in differences of 10–20% in tensile strength between batches, complicating industrial standardization and quality control.

Industrial efforts such as blending scrap from multiple sources and performing chemical composition checks before melting have improved consistency to some extent. Nevertheless, maintaining uniform mechanical properties in recycled aluminum remains a persistent challenge, emphasizing the importance of carefully tailored heat treatment protocols to achieve predictable strength and hardness.

3. Heat Treatment and Microstructure

3.1 Solution Treatment Methods

Solution treatment is a fundamental step in the heat treatment of aluminum alloys, designed to dissolve soluble phases into the aluminum matrix and produce a homogeneous solid solution. In recycled aluminum, the effectiveness of solution treatment is influenced by the chemical variability of the scrap, particularly levels of silicon, copper, and magnesium. Brazilian industrial reports suggest that typical solution treatment temperatures for aluminum alloys range from 500°C to 540°C, with holding times between 1 and 3 hours, depending on the thickness of the material.

During solution treatment, intermetallic compounds such as AlFeSi and Cu-rich phases partially dissolve, while the matrix becomes supersaturated with alloying elements. This process reduces compositional gradients and promotes more uniform precipitation during subsequent aging treatments. However, the heterogeneous nature of recycled aluminum can lead to incomplete dissolution in certain regions, particularly where impurities like iron or zinc are concentrated. These undissolved particles can act as stress concentrators and affect mechanical performance.

Cooling rate after solution treatment also plays a critical role. Rapid quenching, often in water or polymer solutions, preserves the supersaturated solid solution and prevents premature precipitation. Slower cooling, which can occur in industrial furnaces with high thermal mass, may lead to early formation of coarse precipitates, reducing the potential for hardness and tensile strength improvements. Some Brazilian facilities have adopted controlled quenching techniques to balance internal stress development and microstructural uniformity, aiming to reduce warping or cracking in structural components.

Solution treatment thus establishes the foundation for later strengthening during artificial or natural aging. In recycled alloys, understanding the interplay between composition, temperature, and cooling rate is essential, as these parameters determine how effectively the alloy can develop desirable mechanical properties despite the variability inherent in scrap material.

3.2 Artificial and Natural Aging

After solution treatment, aging processes are applied to enhance the mechanical properties of aluminum alloys through controlled precipitation of secondary phases. In recycled aluminum, both artificial and natural aging are commonly used, depending on the desired balance between hardness, tensile strength, and production speed. Artificial aging, also called T6 treatment, typically involves holding the alloy at temperatures between 150°C and 180°C for 4–8 hours. During this period, fine precipitates such as Mg2Si and Cu-rich particles form throughout the matrix, providing significant strengthening through impediment of dislocation motion.

Natural aging occurs at room temperature and generally requires a longer period, ranging from several days to weeks, for the supersaturated solid solution to form precipitates. While slower than artificial aging, natural aging is energy-efficient and can be sufficient for less critical applications, such as window frames or non-structural components. However, recycled alloys with variable copper and magnesium content may show uneven precipitation, leading to local

variations in hardness and tensile strength.

The effectiveness of aging depends heavily on the preceding solution treatment. Alloys with incomplete dissolution of intermetallic compounds or heterogeneous microstructures may develop coarse or unevenly distributed precipitates during aging, reducing the expected strength gains. Brazilian studies indicate that controlling both aging temperature and time is crucial: an excessive aging temperature above 200°C can cause overaging, where precipitates coarsen and tensile strength declines, while insufficient aging time may fail to achieve optimal hardness.

In industrial practice, artificial aging is preferred for components requiring consistent performance, such as automotive engine parts or structural profiles, while natural aging may be applied for non-critical products. Variations in recycled alloy composition require careful adjustment of aging parameters to ensure reproducible mechanical properties, particularly tensile strength and hardness.

3.3 Microstructural Evolution

Microstructural evolution in recycled aluminum alloys during heat treatment is a complex process influenced by alloy composition, prior processing history, and the parameters of solution treatment and aging. Recycled alloys often contain heterogeneous distributions of alloying elements and residual impurities, which directly affect the formation and growth of precipitates, grain structures, and intermetallic phases. During solution treatment, the aim is to dissolve soluble phases into the aluminum matrix, creating a supersaturated solid solution. However, in recycled aluminum, incomplete dissolution can occur in regions with elevated iron or zinc content, resulting in non-uniform microstructures that persist into subsequent aging steps.

During artificial aging, fine precipitates such as Mg2Si and Cu-rich phases nucleate and grow within the supersaturated matrix. These precipitates serve as obstacles to dislocation motion, contributing to increased hardness and tensile strength. In heterogeneous recycled alloys, the nucleation sites for precipitation can be unevenly distributed, leading to localized variations in mechanical properties. Grain boundaries play an additional role; they act as preferential sites for precipitate formation and can influence the coarsening behavior of secondary phases over time.

Natural aging, occurring at room temperature, promotes slower precipitation, which can lead to clusters of solute atoms forming over days to weeks. In alloys with variable composition, such clusters may not be evenly spaced, producing regions of differential hardness or ductility. Moreover, prior mechanical deformation, such as rolling or extrusion, introduces dislocations that can act as additional nucleation sites for precipitates, further complicating the microstructure. Residual stresses from earlier processing can also affect grain morphology and the stability of precipitates, sometimes inducing microcracks in stressed regions.

High-resolution studies, such as scanning electron microscopy (SEM) and transmission electron microscopy (TEM) performed in Brazilian research facilities, show that recycled aluminum microstructures are often more heterogeneous than virgin alloys. Variations in grain size, precipitate density, and the presence of coarse intermetallic particles contribute to the observed scatter in tensile strength and hardness. Controlled heat treatment can partially homogenize these microstructures, but batch-to-batch variations in recycled scrap mean that some degree of heterogeneity is unavoidable.

The evolution of microstructure is therefore a key determinant of mechanical behavior in recycled aluminum alloys. Understanding how grain size, precipitate formation, and residual stress interact provides a theoretical basis for predicting the outcomes of different heat treatment protocols. It also highlights why tailoring heat treatment parameters for specific recycled batches is critical to achieving consistent tensile strength and hardness in industrial applications.

3.4 Impacts on Strength and Hardness

The mechanical performance of recycled aluminum alloys is closely tied to the microstructural changes induced by heat treatment. Solution treatment establishes a uniform supersaturated matrix, which sets the stage for subsequent aging processes to generate fine precipitates that obstruct dislocation motion. In recycled alloys, variability in composition and residual impurities can lead to uneven precipitate distribution, which directly affects tensile strength and hardness. Brazilian industrial studies indicate that tensile strength can vary from 150 to 250 MPa after proper artificial aging, whereas untreated or poorly processed batches

may only achieve 120–140 MPa. Similarly, Vickers hardness typically increases by 15–25% following artificial aging at 160–180°C for 4–6 hours.

Alloying elements play a pivotal role in determining the effectiveness of heat treatment. Magnesium and silicon promote the formation of Mg2Si precipitates, which contribute significantly to hardness and strength. Copper, commonly found in automotive scrap, accelerates precipitation but can also increase sensitivity to overaging if aging time or temperature is excessive. Iron-rich intermetallics, on the other hand, can act as stress concentrators, reducing ductility and potentially offsetting some benefits of precipitate strengthening. These interactions make precise control of heat treatment parameters essential, particularly when recycled alloys are derived from heterogeneous scrap sources.

Residual stress and grain boundary characteristics also influence mechanical properties. Recycled aluminum often contains internal stresses from prior casting or rolling, which can interact with precipitates during aging. In regions of high residual stress, premature microcrack initiation may occur, reducing effective tensile strength despite overall hardness improvements. Grain size heterogeneity further contributes to localized variations, with finer grains generally enhancing strength via the Hall-Petch effect, while coarse or elongated grains may compromise uniformity.

Industrial implications are significant. For structural or automotive components, achieving consistent tensile strength and hardness is critical for safety and reliability. Brazilian manufacturers have observed that tailored heat treatment, considering alloy composition and prior processing history, can reduce property scatter and improve predictability. Experimental studies, literature reviews, and simulation models suggest that even minor adjustments in solution temperature, aging duration, or cooling rate can influence final performance, highlighting the importance of mechanism-based process design in recycled aluminum applications.

4. Mechanisms of Strengthening

4.1 Grain Refinement Effects

Grain refinement is a key mechanism by which heat treatment enhances the mechanical properties of aluminum alloys. In recycled aluminum, heterogeneous microstructures and residual impurities can lead to irregular grain sizes after casting, which directly impacts strength and hardness. Solution treatment followed by controlled cooling promotes more uniform grain structures, reducing coarse dendritic regions that act as weak points under mechanical load. Research in Brazilian facilities indicates that alloys with an average grain size of 15–25 μm exhibit significantly higher tensile strength compared to batches with larger or uneven grains, where strength can drop by up to 20–25%.

The effectiveness of grain refinement is influenced by the presence of alloying elements. Magnesium and silicon contribute to the nucleation of fine grains during solution treatment, while excess iron or residual copper can inhibit uniform grain growth. Dislocation density and prior work history, such as rolling or extrusion, also interact with grain boundaries, enhancing strain-hardening potential in some regions while creating stress concentration in others. In recycled alloys, these effects are compounded by variability in the source material, making the control of thermal parameters critical for achieving consistent microstructures.

Grain refinement contributes to mechanical performance primarily through the Hall-Petch relationship, where smaller grains increase the barrier to dislocation motion, improving yield strength and hardness. In Brazilian recycled alloys, controlled heat treatment has been shown to improve Vickers hardness by 10–20% solely through grain size homogenization, even before accounting for precipitation hardening effects during aging. For tensile performance, refined grains provide more uniform load distribution, reducing the likelihood of localized failure under applied stress.

Industrial observations also highlight the importance of grain size control in automotive and structural applications. Engine components, suspension parts, and load-bearing profiles benefit from uniform grains, which improve fatigue resistance and dimensional stability. In contrast, recycled batches with uneven grain distribution are prone to microcracks and lower overall ductility. This underscores why grain refinement is considered a foundational strengthening mechanism, forming the basis for subsequent processes such as precipitation hardening or artificial aging.

4.2 Precipitation Hardening Mechanisms

Precipitation hardening is one of the most effective methods to enhance the strength and hardness of aluminum alloys. In recycled aluminum, this process depends heavily on the distribution of alloying elements, the presence of residual impurities, and the prior thermal history of the material. During artificial aging, supersaturated solid solutions formed in the preceding solution treatment undergo nucleation and growth of fine precipitates, primarily Mg2Si in Al-Mg-Si alloys and Cu-rich phases in automotive scrap alloys. These precipitates impede dislocation motion, providing substantial increases in tensile strength and hardness.

In Brazilian recycled aluminum, precipitation behavior is influenced by heterogeneous composition. Magnesium content typically varies between 0.3% and 1.2%, while silicon ranges from 0.4% to 1.5%. High copper content in automotive scrap can accelerate the nucleation of precipitates, but excessive copper may also promote coarse particle formation, which reduces overall ductility. Industrial data suggest that well-controlled artificial aging can increase hardness by 15–25% and tensile strength by 20–30% compared to untreated recycled batches. Overaging, however, can occur if temperature or time is too high, leading to coarsened precipitates and a decline in mechanical performance.

The interaction between precipitates and microstructure is critical. Grain boundaries often serve as preferential sites for precipitation, particularly when dislocations or residual stresses are present from prior processing. SEM and TEM studies on Brazilian recycled alloys indicate that areas with higher dislocation density exhibit denser precipitate clusters, which locally enhance hardness but may also create stress concentration points. This heterogeneous precipitation explains why recycled alloys often show variability in mechanical properties, even within the same batch.

Precipitation hardening also interacts with other strengthening mechanisms. Grain refinement from solution treatment enhances the uniform distribution of precipitates, while solid solution effects provide an initial baseline of lattice strengthening. In recycled alloys, residual stress from casting or prior deformation can modify precipitate morphology, sometimes producing elongated or irregular shapes that affect load transfer under tensile stress.

From an industrial perspective, precipitation hardening is essential for components that experience cyclic loading or thermal stress, such as engine blocks, structural frames, or suspension parts. Brazilian automotive plants have adopted carefully controlled aging protocols, balancing time and temperature to maximize tensile strength while minimizing ductility loss. In construction applications, precipitation strengthening ensures consistent hardness in profiles and extrusions, critical for long-term structural performance.

4.3 Solid Solution Strengthening

Solid solution strengthening is a mechanism in which alloying elements dissolve into the aluminum lattice, causing localized lattice distortions that impede dislocation motion. In recycled aluminum alloys, elements such as magnesium, copper, and silicon contribute most significantly to this effect. The concentration and distribution of these elements vary depending on the source of scrap, making solid solution strengthening particularly relevant for recycled batches with heterogeneous compositions.

Magnesium and silicon in Al-Mg-Si alloys create lattice distortions that increase yield strength, while copper enhances this effect by forming coherent clusters within the matrix. Industrial data from Brazilian recycling plants indicate that variations of 0.2–0.5% in magnesium or copper content can lead to 10–15% differences in tensile strength after heat treatment. These effects are compounded by residual impurities; for example, iron-rich intermetallics can interfere with the uniformity of solid solution strengthening by creating regions of stress concentration.

The effectiveness of solid solution strengthening also depends on heat treatment conditions. Solution treatment followed by rapid quenching preserves a supersaturated solid solution, maximizing lattice distortions before aging occurs. Slow cooling or uneven temperature distribution, which can occur in industrial furnaces, allows partial precipitation of solute atoms during cooling, reducing the strengthening potential. Brazilian manufacturers have adopted controlled quenching protocols, often using water or polymer solutions, to maintain uniform lattice distortion across ingots and billets.

Solid solution strengthening interacts with other

mechanisms, particularly precipitation hardening. A well-distributed supersaturated solid solution provides the precursor for fine precipitate nucleation during artificial aging, which further enhances hardness and tensile strength. In recycled aluminum, where composition and prior processing vary, understanding the interplay between solid solution effects and precipitation is critical for achieving consistent mechanical performance. Grain size also influences solid solution effectiveness, as smaller grains increase the proportion of solute atoms near grain boundaries, further impeding dislocation motion and enhancing strength.

From an industrial perspective, solid solution strengthening contributes to mechanical reliability in components exposed to static and cyclic loading, such as engine blocks and structural profiles. Control of alloy composition and quenching conditions allows Brazilian manufacturers to exploit solid solution effects while compensating for heterogeneity in recycled batches, ultimately improving both strength and hardness in the final product.

4.4 Role of Residual Stress

Residual stresses are internal stresses retained in recycled aluminum alloys as a result of prior processing, including casting, rolling, extrusion, or previous thermal cycles. In recycled materials, these stresses are often unevenly distributed due to heterogeneous composition and variable cooling histories, making them an important factor in determining mechanical behavior after heat treatment. Localized tensile or compressive stresses can influence dislocation movement, precipitate formation, and even crack initiation under applied load.

During solution treatment, high residual stresses can partially relax, but regions with coarse intermetallic particles or segregated impurities may retain localized stress concentrations. In Brazilian recycled aluminum, studies have shown that residual stresses in untreated billets can reach 50–80 MPa, particularly near surface regions or areas previously subjected to mechanical work. If not addressed, these stresses can cause warping, dimensional instability, or reduced fatigue life in structural or automotive components.

Artificial aging and natural aging interact with residual stresses in complex ways. Fine precipitates nucleating near dislocations or stressed regions can either relieve or amplify local stresses, depending on the distribution and orientation of the precipitates. For instance, in Al-Mg-Si alloys, dense Mg2Si clusters forming near tensile-stressed zones can locally increase hardness but may also reduce ductility, particularly in recycled batches with uneven element distribution. Control of aging temperature and time is therefore critical to balance strengthening with stress management.

Residual stress also affects grain boundary behavior. Compressive stresses near boundaries can inhibit dislocation motion and improve yield strength, whereas tensile stresses may act as initiation sites for microcracking. SEM studies of Brazilian recycled alloys indicate that areas with high residual stress often correlate with coarse precipitates or microvoids, which explains some of the variability observed in tensile testing across batches.

From an industrial standpoint, controlling residual stresses is essential for components exposed to dynamic loads or thermal cycles. Brazilian automotive and construction manufacturers often implement stress-relief annealing or controlled quenching to reduce detrimental residual stresses, improving mechanical reliability. By understanding the role of residual stress alongside other strengthening mechanisms, heat treatment can be tailored to maximize hardness and tensile performance even in heterogeneous recycled aluminum batches.

5. Literature Insights

5.1 Summary of Global Studies

A significant body of research has explored the effects of heat treatment on recycled aluminum alloys in multiple regions, including Europe, North America, and Asia. In Europe, studies have primarily focused on automotive scrap alloys, highlighting the impact of solution treatment and artificial aging on mechanical performance. For instance, German researchers reported that Al-Mg-Si recycled alloys subjected to solution treatment at 520°C for 2 hours, followed by artificial aging at 175°C for 6 hours, achieved tensile strengths of 220–240 MPa and Vickers hardness values of 70–80 HV, closely matching the performance of virgin alloys with similar composition.

In North America, research has concentrated on beverage can scrap and post-industrial waste. A study from the United States showed that controlled aging of recycled aluminum sheets

could improve hardness by 18–22% compared to untreated sheets, with precipitation hardening playing a dominant role in strengthening. The work also emphasized that variations in silicon content (0.6–1.4%) led to differences in precipitate distribution, resulting in mechanical property scatter. Canadian studies on automotive aluminum components highlighted the interaction between residual stresses and grain refinement, demonstrating that heterogeneous microstructures in recycled material could be partially mitigated through carefully controlled quenching protocols.

Asian research, particularly from China and Japan, has examined the role of multi-step heat treatment in both recycled and mixed aluminum alloys. For example, artificially aged alloys with intermediate temperature holding stages exhibited more uniform precipitation, improving tensile strength consistency across batches. These studies also incorporated microstructural characterization using TEM and SEM, revealing that fine Mg2Si and Cu-rich precipitates were more evenly distributed in alloys with pre-homogenization steps, reducing the variability introduced by heterogeneous scrap.

Several trends emerge from the global literature. Recycled aluminum generally requires higher attention to composition variability than virgin alloys, and industrial heat treatment parameters must often be tailored to the specific batch. Additionally, the combination of solution treatment, controlled quenching, and artificial aging is consistently reported as the most effective strategy to improve both tensile strength and hardness. However, studies frequently note that residual stresses, coarse intermetallic particles, and uneven grain structures remain critical sources of performance variability, regardless of geographic context.

5.2 Comparison with Virgin Alloys

Comparisons between recycled and virgin aluminum alloys highlight both the potential and the limitations of recycled material in industrial applications. Virgin alloys typically exhibit more uniform chemical composition and microstructure, leading to predictable mechanical properties. For example, Al-Mg-Si alloys produced from primary aluminum sources often achieve tensile strengths in the range of 240–260 MPa and Vickers hardness around 75–85 HV after standard T6 treatment, with minimal batch-to-batch variation.

Recycled alloys, in contrast, show wider variability due to heterogeneity in source material. Brazilian studies indicate that even after identical solution treatment and artificial aging, tensile strength can fluctuate between 150 and 250 MPa, and hardness between 60 and 80 HV, depending on scrap origin and impurity content. Automotive scrap, for instance, may contain elevated copper and magnesium levels, improving hardness but potentially introducing coarse intermetallic phases that reduce ductility. Beverage can scrap has more consistent manganese content but may be deficient in other alloying elements, resulting in lower strength after aging.

Global studies emphasize that these differences are largely linked to microstructural uniformity and precipitate distribution. Virgin alloys tend to develop evenly spaced precipitates throughout the matrix, whereas recycled aluminum often exhibits localized clusters or regions with coarse intermetallic particles. SEM and TEM analyses confirm that grain size is more homogeneous in virgin alloys, whereas recycled batches may display elongated or irregular grains due to prior processing histories. These structural differences are reflected in mechanical testing, with recycled alloys showing higher scatter in stress-strain curves and variable fracture behavior.

From an industrial perspective, recycled alloys can approach the performance of virgin materials when heat treatment is carefully controlled and alloying composition is adjusted. For instance, blending recycled batches to standardize magnesium and silicon content, followed by precise solution treatment and artificial aging, can produce tensile strengths within 10–15% of virgin alloy values. Nevertheless, residual impurities such as iron or trace lead remain a limiting factor, occasionally forming stress concentrators or initiating microcracks under applied load.

This comparison underscores that while recycled aluminum can meet many industrial requirements, its mechanical predictability is inherently lower than that of virgin alloys, necessitating careful processing and heat treatment design to achieve consistent hardness and tensile performance.

5.3 Relevance to Brazilian Materials

The performance and processing behavior of recycled aluminum in Brazil are strongly influenced by the country's specific industrial

and scrap sources. Automotive scrap constitutes a large proportion of the recycled material, particularly from domestic vehicle dismantling and industrial component turnover. These alloys often have higher copper and magnesium content compared to consumer packaging scrap, which can enhance precipitation hardening but also increase the risk of coarse intermetallic formation. Brazilian studies report that tensile strength for automotive scrap alloys after standard solution treatment and artificial aging typically ranges between 200 and 240 MPa, while hardness varies from 65 to 78 HV, reflecting batch-to-batch variability.

Industrial scrap from manufacturing and construction processes introduces additional heterogeneity. Aluminum sheets, extrusions, and profiles from previous production cycles may carry residual stresses, minor impurities, or partially dissolved alloying elements. For example, Brazilian plants processing mixed industrial scrap often detect iron content between 0.5% and 1.1%, which can lead to coarse AlFeSi intermetallic particles. These particles act as localized stress concentrators, affecting both tensile strength and fatigue resistance. SEM analyses conducted at Brazilian recycling facilities confirm the presence of uneven precipitate distribution and microvoids in some recycled batches, which partially explains observed variability in mechanical testing.

Brazilian manufacturers have adopted strategies to reduce variability, such as batch blending, pre-melting chemical analysis, and controlled quenching protocols. In some cases, blending multiple scrap sources allows Mg and Si content to be standardized, which improves the predictability of precipitate formation during aging. Controlled quenching from solution treatment temperatures around 520–530°C ensures a more uniform supersaturated solid solution, maximizing the potential for precipitation hardening. Despite these efforts, complete uniformity remains challenging, particularly when dealing with mixed automotive and industrial scrap.

Environmental factors and regional industrial practices also influence recycled aluminum properties. In coastal states such as Rio de Janeiro, exposure to high humidity and salinity during storage can induce surface oxidation, necessitating careful fluxing during remelting to avoid oxide entrapment. Similarly, Brazilian facilities processing high volumes of beverage cans report that even minor deviations in melt temperature or cooling rate can create localized variations in hardness across ingots. These observations underscore that heat treatment strategies must be specifically tailored for Brazilian recycled alloys, taking into account both composition heterogeneity and industrial process conditions.

5.4 Knowledge Gaps and Open Questions

Despite the growing body of literature on recycled aluminum alloys, significant knowledge gaps remain, particularly regarding the mechanisms of heat treatment in heterogeneous Brazilian materials. While global studies provide insight into solution treatment, aging, and precipitation effects, few investigations focus specifically on the variability of Brazilian scrap sources and their impact on mechanical properties. Automotive scrap, industrial waste, and beverage can alloys all exhibit distinct chemical compositions and prior processing histories, yet systematic studies comparing these sources under identical heat treatment conditions are limited.

Another gap concerns the interaction of multiple strengthening mechanisms in recycled alloys. Grain refinement, solid solution strengthening, precipitation hardening, and residual stress effects have been studied individually, but integrated analyses that quantify how these mechanisms interact in heterogeneous batches are scarce. Brazilian recycled aluminum often contains impurities such as iron, zinc, or lead, which influence precipitate morphology and grain boundary behavior, but detailed microstructural characterization studies linking these impurities to mechanical variability remain underexplored.

Process variability also presents challenges for predictive modeling. Most thermomechanical simulations are based on homogeneous or virgin alloys, which do not accurately represent the heterogeneity found in Brazilian recycled materials. The lack of reliable predictive models for tensile strength, hardness, and fatigue performance limits industrial optimization of heat treatment protocols. Furthermore, experimental data on long-term durability and performance under cyclic loading or environmental exposure is sparse, leaving questions about the reliability of recycled aluminum in structural applications.

Finally, sustainability and lifecycle

considerations are underrepresented in current research. While energy savings from recycling are well documented, studies examining the trade-offs between heat treatment intensity, mechanical performance, and environmental impact are limited. Brazilian industries increasingly face pressures to optimize both material properties and ecological footprint, yet empirical or theoretical guidance for balancing these factors is lacking.

Addressing these gaps will require integrated studies that combine microstructural analysis, mechanical testing, industrial process monitoring, and modeling. Understanding the interplay between alloy composition, heat treatment, and residual impurities is essential for achieving consistent mechanical performance in Brazilian recycled aluminum.

6. Industrial Relevance

6.1 Automotive Applications

Automotive applications are the primary industrial outlet for recycled aluminum in Brazil. Recycled alloys are used in engine components, transmission housings, suspension elements, and body panels due to their favorable strength-to-weight ratio, corrosion resistance, and cost-effectiveness. For example, some Brazilian assembly plants in São Paulo report incorporating over 15,000 tons of recycled aluminum annually, representing a significant proportion of non-ferrous material in vehicle production.

The performance requirements for automotive components are stringent. Engine blocks and transmission housings must maintain high tensile strength and dimensional stability under thermal cycling, while body panels and suspension parts are subject to repeated mechanical loads and fatigue. Heat treatment plays a crucial role in meeting these specifications. Solution treatment followed by artificial aging ensures uniform precipitation of Mg2Si and Cu-rich phases, increasing both hardness and tensile strength. Variability in recycled material composition, however, necessitates adjustments in heat treatment parameters to achieve consistent mechanical properties.

Residual stresses and heterogeneous microstructures can significantly affect fatigue performance. Brazilian recycled alloys often retain stress concentrations from prior casting, extrusion, or rolling, which may serve as crack initiation sites under cyclic loading. Controlled quenching protocols and precise aging schedules are therefore implemented to mitigate these effects. For instance, a study on recycled Al-Mg-Si engine components reported that adjusting artificial aging time by 30–60 minutes could reduce variability in tensile strength by up to 15% across different batches.

In addition to mechanical performance, industrial processing constraints such as throughput, energy consumption, and component size influence heat treatment strategies. Large structural components require slower heating and quenching to minimize thermal gradients, whereas smaller parts can be aged more rapidly. Brazilian manufacturers have begun using process simulation and thermal monitoring to optimize these parameters, balancing mechanical performance with efficiency and cost.

Finally, the integration of recycled aluminum into automotive supply chains is increasingly tied to sustainability targets. By improving the predictability of mechanical properties through tailored heat treatment, manufacturers can replace virgin aluminum with recycled material without compromising component reliability, contributing to reduced carbon emissions and energy consumption across vehicle production.

6.2 Construction and Lightweight Components

Recycled aluminum alloys are widely used in the construction sector in Brazil, particularly for structural profiles, roofing, curtain walls, and window frames. Coastal and tropical regions, including Rio de Janeiro and São Paulo, present challenging environmental conditions such as high humidity and salt-laden air, which make corrosion resistance a key consideration. Aluminum alloys from recycled sources, when properly treated, offer adequate durability and long service life for these applications. Brazilian manufacturers report that structural profiles produced from recycled aluminum exhibit Vickers hardness values between 60 and 75 HV, sufficient to meet local building codes and safety standards.

The variability in recycled aluminum composition requires careful control of heat treatment to ensure consistent performance. Alloys derived from automotive scrap, which may contain elevated magnesium and copper, provide higher potential strength, but coarse intermetallic phases can form during aging if the

material is not properly processed. Industrial facilities mitigate this risk through controlled solution treatment, precise quenching, and aging schedules tailored to the source material. For larger profiles and panels, temperature gradients during heating and cooling are monitored to avoid warping and uneven microstructure formation.

Lightweight components, such as prefabricated building elements and façade panels, benefit from the low density of aluminum, which reduces structural load while maintaining mechanical stability. In these cases, tensile strength requirements are lower than for automotive components, but uniform hardness across the component is critical to prevent local deformation during installation. Some Brazilian producers have implemented real-time thermal monitoring and post-processing inspection using hardness testing across the length of extrusions to ensure uniformity.

In addition to structural performance, recycled aluminum's environmental advantages are increasingly important in construction projects pursuing sustainability certifications. By replacing primary aluminum with recycled material, Brazilian manufacturers reduce energy consumption and CO2 emissions, while achieving mechanical performance sufficient for long-term durability. Heat treatment protocols are designed not only to maximize tensile strength and hardness but also to maintain dimensional stability during fabrication and long-term service.

6.3 Heat Treatment Optimization for Industry

Optimizing heat treatment for recycled aluminum in industrial applications requires careful consideration of alloy composition, residual impurities, and component geometry. Brazilian facilities processing automotive and industrial scrap have developed protocols that combine solution treatment, controlled quenching, and artificial aging to achieve predictable tensile strength and hardness. Solution treatment temperatures are generally maintained between 520°C and 530°C, with holding times of 1.5 to 3 hours, depending on component thickness. Quenching is performed in water or polymer solutions to preserve supersaturation and promote uniform precipitate formation during aging.

Aging parameters are adjusted according to the specific source of recycled aluminum. Automotive scrap with higher copper content benefits from slightly lower aging temperatures (160–170°C) for 4–6 hours to prevent overaging and coarsening of precipitates. In contrast, beverage can scrap, with more uniform manganese levels, can tolerate higher aging temperatures without compromising ductility. Brazilian manufacturers often monitor batch composition and adjust aging schedules dynamically, using real-time temperature measurement and hardness testing to ensure consistent mechanical performance.

Industrial constraints, including component size, production throughput, and energy consumption, also influence optimization strategies. Large extrusions or structural profiles require careful control of thermal gradients to avoid uneven precipitation and warping. Smaller components can be aged more rapidly, but uniformity is monitored through periodic sampling and hardness measurements along the component length. Some plants have integrated computer-controlled thermal management systems that adjust furnace temperatures and quenching timing based on component geometry and batch composition.

Residual stress management is a critical part of heat treatment optimization. Recycled aluminum often retains stresses from prior casting, rolling, or extrusion. Adjustments to quenching rate and aging duration can mitigate stress concentrations, reducing the risk of microcracking and improving fatigue performance. In Brazilian automotive plants, these adjustments have led to more predictable tensile strength across batches, with observed variability reduced by approximately 10–15%.

Finally, sustainability considerations increasingly shape heat treatment optimization. Minimizing energy use while achieving mechanical targets is a priority, particularly for construction and lightweight applications. By fine-tuning heat treatment schedules based on scrap composition and component requirements, Brazilian manufacturers are able to balance mechanical performance with energy efficiency, producing recycled aluminum components that meet both technical and environmental standards.

7. Challenges and Future Research

7.1 Material Heterogeneity Limitations

Material heterogeneity remains a significant limitation for Brazilian recycled aluminum

alloys. The chemical composition of scrap varies widely depending on the source, with automotive end-of-life components typically containing higher copper and magnesium, while industrial scrap shows more variable iron and zinc levels. Such variability directly affects microstructure uniformity, including grain size, precipitate distribution, and the presence of intermetallic phases. Industrial tensile testing of recycled batches has demonstrated strength variations of up to 20–25% between different sources, even under identical heat treatment protocols.

Residual impurities further complicate processing. Iron-rich intermetallics and trace lead inclusions act as stress concentrators, reducing ductility and potentially initiating microcracks during mechanical loading. Observations from Brazilian manufacturing plants indicate that these microstructural inconsistencies are more pronounced in thicker components or large structural profiles, where thermal gradients during solution treatment and quenching amplify heterogeneity effects.

The influence of prior mechanical processing also contributes to heterogeneity. Recycled aluminum that has undergone multiple casting, rolling, or extrusion cycles often retains residual stresses and dislocations, leading to uneven precipitation during aging. These localized variations in hardness and tensile strength are particularly critical in automotive and structural components, where consistent mechanical performance is essential for safety and reliability.

Industrial strategies to mitigate material heterogeneity include blending scrap from multiple sources, pre-melting chemical analysis, and tailored heat treatment schedules. While these approaches improve overall consistency, absolute uniformity is difficult to achieve. The combination of variable alloying elements, residual impurities, and prior processing history ensures that material heterogeneity will remain a persistent challenge for Brazilian recycled aluminum.

7.2 Mechanistic Modeling Approaches

Mechanistic modeling plays a crucial role in predicting the performance of recycled aluminum alloys, but its application to heterogeneous Brazilian materials remains limited. Most computational models are developed for homogeneous or virgin alloys, assuming uniform composition and microstructure. These models can effectively simulate dislocation movement, precipitation kinetics, and grain boundary strengthening, but they often fail to account for the variability inherent in recycled scrap.

For Brazilian alloys, where iron, copper, magnesium, and silicon contents vary significantly between batches, mechanistic models must incorporate composition-dependent parameters. Variations in alloying elements affect precipitate nucleation rates, growth kinetics, and solid solution strengthening, which are critical for accurate predictions of tensile strength and hardness. Studies from São Paulo and Minas Gerais suggest that neglecting these variables can result in predictive errors of 15–20% when estimating mechanical properties under standard heat treatment conditions.

Residual stresses and microstructural heterogeneity further complicate modeling. Finite element simulations indicate that stress concentrations around coarse intermetallic particles can accelerate local deformation and crack initiation, yet few models integrate these localized effects with macroscopic property predictions. Additionally, the interaction between grain refinement, precipitation hardening, and solid solution strengthening is often simplified, ignoring the complex interdependence observed in recycled aluminum.

Industrial implementations have begun integrating modeling with real-time process control. Some Brazilian plants use simulation data to adjust solution treatment temperatures, quenching rates, and aging durations based on the measured composition of each scrap batch. These adjustments improve property uniformity and reduce the risk of failure in critical components, particularly in automotive engine blocks and structural profiles. However, the lack of validated, comprehensive models for heterogeneous recycled aluminum remains a key limitation, restricting predictive capability and optimization potential.

Advancing mechanistic modeling for Brazilian recycled alloys requires combined efforts in microstructural characterization, computational simulation, and industrial validation. Incorporating localized impurity effects, residual stresses, and batch-specific composition data into predictive frameworks could enhance the

accuracy of strength and hardness predictions, guiding both heat treatment and component design in industrial practice.

7.3 Sustainability and Environmental Considerations

Sustainability is a central consideration in the Brazilian recycled aluminum industry. Recycling aluminum consumes only 5–10% of the energy required to produce primary aluminum, significantly reducing greenhouse gas emissions. The widespread adoption of recycled aluminum in automotive, construction, and packaging applications contributes to national and corporate carbon reduction goals. Energy savings are further enhanced when optimized heat treatment processes are applied, minimizing excessive thermal exposure while achieving target mechanical properties.

Environmental constraints influence industrial processing decisions. For example, rapid quenching in water requires substantial energy for water circulation and temperature control, while polymer-based quenching solutions involve considerations of chemical disposal and reuse. Brazilian facilities have implemented closed-loop cooling systems and water treatment processes to reduce environmental impact, particularly in regions where water scarcity is a concern.

The variability inherent in recycled aluminum also intersects with sustainability goals. Alloy batches that require additional heat treatment cycles due to inconsistent composition or impurities consume more energy and generate higher emissions. Studies from industrial plants indicate that blending scrap batches and implementing precise compositional analysis prior to heat treatment can reduce the number of repeat cycles by 10–15%, directly lowering energy usage and associated environmental impact.

Material efficiency is another important factor. High scrap heterogeneity can lead to rejected batches or components that fail quality inspections, increasing waste generation. Industrial strategies in Brazil include monitoring hardness and tensile strength across multiple points in each batch and selectively remelting underperforming portions. These measures improve material utilization and reduce overall scrap waste, aligning production with circular economy principles.

Sustainability considerations also extend to lifecycle performance. Components made from recycled aluminum must maintain mechanical reliability over years of service to prevent premature replacement or repair, which would offset the environmental benefits of recycling. Brazilian engineering standards increasingly require assessments of long-term durability, emphasizing the combined role of heat treatment and material composition in ensuring both performance and environmental efficiency.

7.4 Recommendations for Future Studies

Future research on recycled aluminum alloys in Brazil should focus on addressing the variability inherent in scrap materials and improving predictive capability for mechanical performance. One priority is developing integrated mechanistic models that combine microstructural evolution, residual stress distribution, and precipitation kinetics. Such models would allow manufacturers to anticipate tensile strength and hardness outcomes for specific batches, reducing reliance on trial-and-error adjustments in heat treatment protocols.

Expanded microstructural characterization is also critical. High-resolution techniques, including TEM and SEM, can provide detailed information on precipitate morphology, grain boundary behavior, and the distribution of residual impurities. These data can inform both computational models and industrial processing decisions, particularly in automotive and structural applications where component reliability is essential. Quantitative analysis of grain size distribution and intermetallic particle density could improve understanding of performance variability across recycled batches.

Another area of research involves optimizing heat treatment protocols tailored to heterogeneous Brazilian scrap. Investigations could explore multi-step aging, variable quenching rates, or hybrid thermal cycles to enhance mechanical properties while minimizing energy consumption. Industrial trials comparing different alloy sources, processing histories, and treatment parameters would provide practical guidance for scaling laboratory findings to production environments.

Sustainability-oriented studies should also be prioritized. Assessing the trade-offs between mechanical performance, energy use, and environmental impact will help manufacturers develop heat treatment strategies that maximize both material properties and ecological efficiency. Life-cycle analysis of recycled

aluminum components under real-world service conditions could guide decision-making for automotive and construction sectors, ensuring durability while reducing carbon footprint.

Finally, establishing standardized testing protocols and data sharing across Brazilian recycling facilities could improve the consistency of recycled aluminum performance. Collaborative research initiatives between industry and academia would facilitate benchmarking, enabling identification of best practices in heat treatment, quality control, and material selection.

8. Conclusion

8.1 Summary of Key Mechanisms

Heat treatment influences tensile strength and hardness in recycled aluminum alloys through a combination of microstructural mechanisms. Solution treatment produces a supersaturated solid solution, which provides the foundation for subsequent strengthening. Grain refinement resulting from controlled solution treatment enhances yield strength by increasing the barrier to dislocation motion. Precipitation hardening, primarily through Mg2Si and Cu-rich phases, obstructs dislocations and contributes to hardness and tensile improvements. Solid solution strengthening introduces lattice distortions that further impede dislocation movement, while residual stresses interact with grain boundaries and precipitates, influencing local mechanical behavior.

In Brazilian recycled aluminum, variability in alloy composition and prior processing modifies how these mechanisms operate. Automotive scrap alloys, with higher copper and magnesium content, can achieve higher hardness and strength through precipitation and solid solution effects, whereas industrial scrap with elevated iron or residual impurities may limit the effectiveness of these mechanisms. Microstructural heterogeneity, including uneven grain sizes and localized precipitate clusters, affects how uniformly the material responds to heat treatment.

These mechanisms collectively determine the mechanical performance of recycled aluminum in industrial applications. Controlled heat treatment can mitigate the influence of heterogeneity, optimize strength and hardness, and improve fatigue resistance for automotive components, structural profiles, and lightweight construction elements. Understanding the interplay of these mechanisms is essential for tailoring heat treatment parameters to the composition and processing history of each recycled batch.

8.2 Theoretical Insights for Brazil

Recycled aluminum alloys in Brazil display characteristics distinct from those reported in studies of homogeneous or virgin materials. Variability in source composition, including automotive, industrial, and consumer scrap, creates microstructural heterogeneity that influences the effectiveness of traditional heat treatment approaches. Understanding the interplay between solution treatment, precipitation hardening, solid solution strengthening, and residual stresses is essential to predict mechanical performance in Brazilian alloys.

Data from Brazilian industrial facilities indicate that alloys with higher magnesium and copper content exhibit more pronounced precipitation hardening effects, enhancing both tensile strength and hardness. Conversely, batches with elevated iron or residual zinc often show localized stress concentrations and coarse intermetallic phases that reduce ductility. Mechanistic models incorporating these variations allow better predictions of strength and hardness across heterogeneous batches, enabling optimization of heat treatment parameters to suit the specific composition of each recycled batch.

Microstructural studies further highlight the influence of grain size and precipitate distribution on mechanical properties. Fine grains, promoted through controlled solution treatment, provide a uniform matrix that supports consistent precipitation, while coarse or elongated grains resulting from heterogeneous scrap can lead to uneven hardness and localized weakness. These insights suggest that predictive models for Brazilian recycled alloys must account not only for overall composition but also for spatial variability within ingots and extrusions.

Industrial experience in Brazil reinforces these theoretical observations. Adjusting aging temperature and duration according to scrap origin improves performance uniformity, and careful quenching mitigates residual stresses that might otherwise reduce tensile strength. Combining microstructural understanding with batch-specific process control provides a practical framework to harness the reinforcing

mechanisms of heat treatment while compensating for the inherent heterogeneity of recycled materials.

8.3 Implications for Industrial Practice

The insights gained from understanding the mechanisms of heat treatment have direct implications for Brazilian industrial applications of recycled aluminum. Tailoring solution treatment temperatures and holding times according to the specific alloy composition can optimize the supersaturation of alloying elements, ensuring consistent nucleation of precipitates during aging. Controlled quenching strategies are critical to reduce residual stresses, which otherwise lead to localized hardness variations or microcracking in structural and automotive components.

Automotive manufacturers can leverage these theoretical insights to improve the predictability of tensile strength and fatigue performance in engine components, body panels, and suspension elements. For example, adjusting aging duration by 30–60 minutes based on the magnesium and copper content of a batch has been shown to reduce strength variability by 10–15% in Brazilian production facilities. Construction and lightweight structural applications also benefit from precise control of heat treatment parameters, ensuring uniform hardness and dimensional stability in extrusions and panels.

Process monitoring and real-time adjustments are increasingly feasible with modern thermal management systems. Brazilian plants have adopted continuous temperature sensors and automated quenching controls to account for variations in scrap composition. These practices minimize performance scatter and improve material utilization, reducing the number of rejected components and waste generated during production.

Additionally, understanding the interaction between microstructure, residual stress, and precipitate distribution supports maintenance of long-term durability. Components exposed to cyclic loads or thermal fluctuations, such as building profiles in coastal environments, require uniform mechanical performance over extended service periods. Integrating theoretical knowledge into industrial practice enables more reliable product performance while supporting sustainability goals by reducing energy consumption and maximizing the use of recycled materials.

References

Chen, X., Ben Saada, M., Lavisse, B., & Ammar, A. (2025). Recent advances in the remelting process for recycling aluminium alloy chips: A critical review. *International Journal of Material Forming, 18*, 42.

Costa, F. R., Almeida, L. M., & Rocha, P. A. (2019). Influence of residual stress on the fatigue behavior of recycled aluminum automotive components. *International Journal of Fatigue, 125*, 208–217.

Effect of continuous casting and heat treatment parameters on the microstructure and mechanical properties of recycled EN AW 2007 alloy (2024). *PubMed Central*.

Figueiredo, L. M., & Oliveira, R. P. (2021). Mechanical performance of recycled Al-Mg-Si alloys under artificial aging. *Journal of Materials Processing Technology, 288*, 116838.

Fujiyama, R. T., & Darwish, F. A. I. (2008). Recycled aluminum: Mechanics and microstructural characterization (SAE Technical Paper 2008-36-0090).

Improving the performance of recycled EN 45500: A sustainable approach through heat treatment optimization. (2026). *Journal of Cleaner Production, 544*, 147718.

Martins, H. C., & Oliveira, T. S. (2021). Heat treatment optimization for heterogeneous aluminum alloys in industrial practice. *Journal of Manufacturing Processes, 64*, 1110–1118.

Mrówka-Nowotnik, G., Boczkal, G., & Nabel, D. (2025). Kinetics of precipitation hardening phases in recycled 2017A aluminum alloy. *Materials, 18*(6), 1235. https://doi.org/10.3390/ma18061235

Mrówka-Nowotnik, G., Gancarczyk, K., Nowotnik, A., Dychtoń, K., & Boczkal, G. (2020). Microstructure and properties of as cast and heat treated 2017A aluminium alloy obtained from scrap recycling. *Materials, 14*(1), 89.

Rady, M. H., Mahdi, A. S., Mustapa, M. S., et al. (2019). Effect of heat treatment on tensile strength of direct recycled aluminium alloy (AA6061). *Materials Science Forum, 961*, 80–87.

Rady, M. H., Mustapa, M. S., Wagiman, A.,

Al-Alimi, S., Shamsudin, S., Lajis, M. A., et al. (2020). Effect of the heat treatment on mechanical and physical properties of direct recycled aluminium alloy (AA6061). *International Journal of Integrated Engineering, 12*(3), 82–89.

Recycled AlSi7Mg0.3 alloys with different iron content: Heat treatment and tensile properties. (2026). *X Materials*.

Rodrigues, A. L., & Gomes, E. P. (2018). Grain refinement and strengthening mechanisms in recycled Al alloys. *Metallurgical and Materials Transactions A, 49*(5), 2074–2085.

Santos, R. F., & Barbosa, J. T. (2020). Sustainability assessment of recycled aluminum production in Brazil. *Resources, Conservation & Recycling, 161*, 104929.

Silva, J. A., Santos, M. F., & Pereira, D. R. (2020). Microstructural evolution in recycled aluminum alloys: A Brazilian perspective. *Materials Science and Engineering A, 789*, 139572.